Status of LHCb Upgrade I

CERN-RRB-2020-036

29 April 2020

Contents

1 Introduction

The LHCb experiment completed its data taking in 2018 and the installation phase of the Upgrade is now in full swing. The upgraded detector will be able to read out all sub-detectors at 40 MHz and to select physics events of interest by means of a pure software trigger at the bunch crossing rate of the LHC. This capability will allow the experiment to collect data with high efficiency at a luminosity of $2 \times 10^{33}\,\mathrm{cm}^{-2}\mathrm{s}^{-1}$. Flavour-physics measurements will be performed with much higher precision than is possible with the previous detector, and across a wider range of observables. The flexibility inherent in the new trigger scheme will also allow the experiment to further diversify its physics programme into important areas beyond flavour.

The Upgrade was proposed in the Letter of Intent [1] in 2011, and its main components and cost-envelope were defined in the Framework TDR [2] one year later. Technical Design Reports (TDRs) have been written for all sub-detector systems as well as for the Software and Computing and the Computing Model [3–8] and approved by the Research Board.

Addenda to the Memorandum of Understanding (MoU) were presented to the RRB in April and October 2014, covering the division of resources and responsibilities for Common Project items [9] and sub-system items [10], respectively. A new sub-project, the Real-Time Analysis Project has been created to organize the complex software developments for the upgrade trigger.

The first part of this document (Sect. 2 and 3) gives a summary of major physics results and operational aspects concerning Run 1 and Run 2 data processing. A total of 10 fb^{-1} were delivered to LHCb in Run 1 + Run 2 data taking periods, with 9 fb^{-1} recorded. The LHCb Run 1 + Run 2 dataset comprises p-p, p-Pb, and Pb-Pb at various centre-of-mass energies, as well as p-A (A = He, Ne, Ar) collisions in fixed target mode, using the unique experiment's gas injection system. The overall operational efficiency was 90% and all sub-detectors operated in a very stable way. Exploitation of Run 1 + Run 2 data is progressing very well with a total of 515 papers published or submitted, of which 9 were submitted in 2020 at the time of writing. Data processing is also proceeding smoothly, with a full Run 1 + Run 2 data reprocessing that will be completed by the end of April.

Physics highlights since the last report include the measurement of the time-dependent CP asymmetry A_Γ in D-meson decays, sensitive to additional sources of CP violation in charm, the first measurement of $|V_{cb}|$ with B_s^0 decays, an updated angular analysis of rare decays $B^0 \to K^{*0}\mu^+\mu^-$, a test of lepton flavour universality in baryons, using the decay $\Lambda_b^0 \to pK^-\ell^+\ell^-$ for $\ell = \mu, e$, the search for very rare decays $B^0_{(s)} \to e^+e^-$, and the observation of several Ω_b resonances. These and other results are discussed in Sect. 3.

In the second part (Sect. 4, 5, 6, 7, 8, 9) an update on the status of the Upgrade is given, reiterating the detector choices made in the TDRs and summarising progress since the previous RRB. All sub-detector and common projects are progressing and are on schedule for the installation deadline, although some areas of concern are present in some of the sub-projects.

Finally, in Sect. 10 and Sect. 11 a brief update on the latest developments on the Upgrade II planning and on collaboration matters is given.

This report has been prepared before the enforcement of many restrictions due to the covid-19 emergency. At the time of submission all the LHCb upgrade construction activities are suspended. Full evaluation of the impact of this stop is ongoing

2 Operations

2.1 Data processing

The re-processing of the data collected during Run 1 and Run 2 for proton-proton collisions is completed. In the re-processing step new or updated selections needed for some physics analyses are applied. For 2015 and 2016 data, updated selections are applied to all the physics analyses to profit of the latest and more accurate calibration of the Calorimeter.

Simulation samples are essential for the validation of physics measurements and to evaluate the associated systematic errors. Very large simulation productions are needed to achieve the high precision measurements of the ambitious LHCb physics programme. These requests are constantly growing and are using the largest fraction (almost 90%) of the total computing power. Efforts are ongoing in the LHCb experiment to provide multiple options for simulating events in a faster way, in particular when high statistics is needed. Two examples of these techniques are to simulate selectively only the elements of the detector essential in a particular measurement or to simulate only particles from the decay of the signal particle while re-using the simulation of the underlying event multiple times. In 2019, about a factor 2 more MC events were produced thanks to the wider use of the fast simulation. Figure 1 (left) shows the number of simulated events per year. To profit from the resources available and to boost the Monte Carlo production, the online-farm is fully used for simulation jobs during this period without data taking. This results in about 40% of Monte Carlo events being produced on the online-farm. Figure 1 (right) shows the jobs running on the online farm in the last year.

2.2 Computing

The usage of computing resources for 2019 [11] and the estimates of computing requirements for 2021 [12] are discussed in detail in separate documents. The LHCb Computing Model for the Upgrade era and the associated computing requirements are presented in [13].

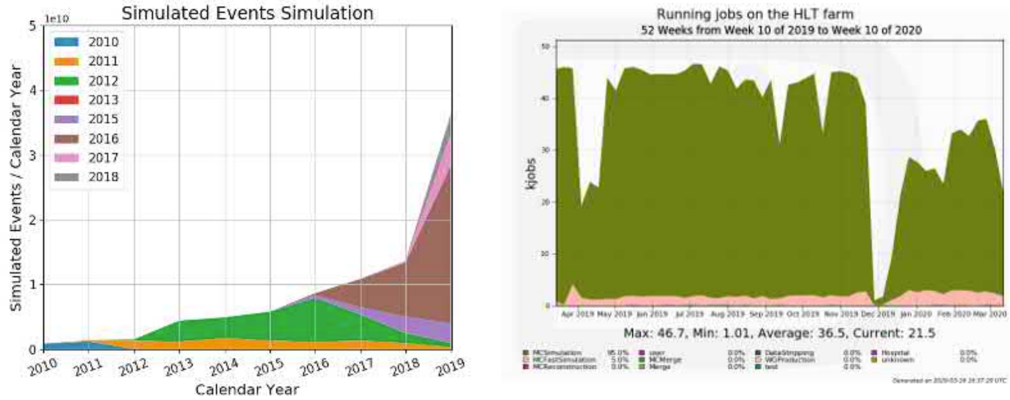

Figure 1: Left: The number of simulated events for physics analysis of Run 1 and Run 2 data as a function of the year. The colors indicate the year of the data-set corresponding to the produced MC sample. Right: The number of jobs run on the online-farm during the last year: pink area indicates Monte Carlo jobs using a fast simulation technique, green area Monte Carlo jobs using the full event simulation.

3 Physics

Since the last RRB report, the LHCb collaboration has submitted 23 new papers, for a total of 515 publications at the time of writing. LHCb has also submitted one conference note. A summary of these is given in Table 1. A further 7 papers are being processed by the LHCb Editorial Board and are close to submission. In the following, some selected results from recent publications are highlighted.

3.1 *CP* violation and CKM studies

The existence of direct *CP* violation in the charm system is now established. However, mixing-induced *CP*-violation in charm decays remains an open question. In the SM, it is predicted to be considerably smaller, at the level of few $\times$ 10^{-5}, and is under better theoretical control than direct CPV. It therefore serves as a sensitive probe for new physics. In [14], LHCb published the results of a search for time-dependent *CP* violation using the A_Γ observable. Experimentally, this is accessed as $A_{CP}(D^0 \to f; t) = A_{CP}^{\rm dir}(f) - A_\Gamma(f)\frac{t}{\tau}$ for a final state f, where $A_{CP}^{\rm dir}$ is the direct *CP* asymmetry, and τ is the average lifetime of D^0 mesons. Thus, by measuring the asymmetry as a function of decay time t, the indirect component can be separated from time-independent effects (which include the direct *CP* asymmetry but also nuisance effects such as the production asymmetry and most detector effects). This analysis uses secondary D^0 mesons (*i.e.* those produced in semileptonic decays of B mesons), for which the decay time acceptance is easier to model than promptly produced charm, and includes the 2016–18 dataset. A precision of better than 10^{-3} is obtained for each decay mode. Combined with results from Run 1, these yield $A_\Gamma(K^+K^-) = (-4.4 \pm 2.3 \pm 0.6) \times 10^{-4}$ and

Table 1: Papers submitted for publication since the previous RRB report.

PAPER-2019-029	Search for the doubly charmed baryon Ξ_{cc}^{+}
PAPER-2019-031	Search for $A' \to \mu^+\mu^-$ decays
PAPER-2019-020	Measurement of f_s/f_u variation with proton-proton collision energy and kinematics
PAPER-2019-035	Measurement of Ξ_{cc}^{++} production in pp collisions at $\sqrt{s} = 13$ TeV
PAPER-2019-033	Measurement of the B_c^- meson production fraction and asymmetry in 7 and 13 TeV pp collisions
PAPER-2019-032	Updated measurement of decay-time-dependent CP asymmetries in $D^0 \to K^+K^-$ and $D^0 \to \pi^+\pi^-$ decays
PAPER-2019-024	Measurement of the $\eta_c(1S)$ production cross-section in pp collisions at $\sqrt{s} = 13$ TeV
PAPER-2019-027	Determination of quantum numbers for several excited charmed mesons observed in $B^- \to D^{*+}\pi^-\pi^-$ decays
PAPER-2019-034	Observation of the semileptonic decay $B^+ \to p\bar{p}\mu^+\nu_\mu$
PAPER-2019-037	Precision measurement of the Ξ_{cc}^{++} mass
PAPER-2019-039	Isospin amplitudes in $\Lambda_b^0 \to J/\psi\Lambda(\Sigma^0)$ and $\Xi_b^0 \to J/\psi\Xi^0(\Lambda)$ decays
PAPER-2019-036	Measurement of CP violation in $B^0 \to D^{*\pm}D^{\mp}$ decays
PAPER-2019-040	Test of lepton universality with $\Lambda_b^0 \to pK^-\ell^+\ell^-$ decays
PAPER-2019-028	Search for CP violation and observation of P violation in $\Lambda_b^0 \to p\pi^-\pi^+\pi^-$ decays
PAPER-2019-042	First observation of excited Ω_b^- states
PAPER-2019-041	Measurement of $\|V_{cb}\|$ with $B_s^0 \to D_s^{(*)-}\mu^+\nu_\mu$ decays
PAPER-2019-038	Strong constraints on the $K_{\mathrm{S}}^0 \to \mu^+\mu^-$ branching fraction
PAPER-2019-045	Observation of a new baryon state in the $\Lambda_b^0\pi^+\pi^-$ mass spectrum
PAPER-2019-030	Measurement of the branching fraction of the decay $B_s^0 \to K_S^0K_S^0$
PAPER-2019-044	Measurement of CP observables in $B^\pm \to DK^\pm$ and $B^\pm \to D\pi^\pm$ with $D \to K_S^0K\pi$ decays
PAPER-2020-001	Search for the rare decays $B_s^0 \to e^+e^-$ and $B^0 \to e^+e^-$
PAPER-2019-043	Search for the lepton flavour violating decay $B^+ \to K^+\mu^-\tau^+$ using B_{s2}^{*0} decays
PAPER-2020-002	Angular analysis of the $B^0 \to K^{*0}\mu^+\mu^-$ decay using $4.7\,\mathrm{fb}^{-1}$ of integrated luminosity
CONF-2019-003	Measurement of Z production cross-sections in proton-lead collisions at $\sqrt{s_{\mathrm{NN}}} = 8.16$ TeV
CONF-2019-004	Study of prompt D^0 meson production in pPb at $\sqrt{s_{\mathrm{NN}}} = 8.16$ TeV at LHCb
CONF-2019-005	Multiplicity-dependent modification of $\chi_{c1}(3872)$ and $\psi(2S)$ production in pp collisions at $\sqrt{s}= 8$ TeV

$A_\Gamma(\pi^+\pi^-) = (2.5 \pm 4.3 \pm 0.7) \times 10^{-4}$. Finally, assuming A_Γ to be independent of the decay mode, an average of $A_\Gamma = (-2.9 \pm 2.0 \pm 0.6) \times 10^{-4}$ is obtained.

In [15], an analysis of time-dependent *CP* violation in $B^0 \to D^{*\pm}D^{\mp}$ decays is reported, using the full LHCb Run1–2 dataset. Mixing-induced CPV in the B system has been studied extensively in $b \to c\bar{c}s$ decay modes such as the golden mode $B^0 \to J/\psi K^0_S$. For $b \to c\bar{c}d$ modes such as $B^0 \to D^{*\pm}D^{\mp}$, the same CKM phase β enters; however, additional diagrams can contribute, potentially introducing further contributions. In this analysis, LHCb measures an extended set of five *CP*-violating observables (S_{D^*D}, ΔS_{D^*D}, C_{D^*D}, ΔC_{D^*D}, A_{D^*D}). Within the current precision, S_{D^*D} is measured to be $-0.861 \pm 0.077 \pm 0.019$, compatible with $-\sin 2\beta$, and the remaining four observables are compatible with zero. This behaviour is expected in the limit that the penguin contribution is negligible and that the processes $B^0 \to D^{*+}D^-$ and $B^0 \to D^{*-}D^+$ have the same magnitude and hadronic phase.

The angle γ of the CKM unitarity triangle is constrained not by a single, dominant measurement but by a combination of numerous, complementary measurements. In [16], LHCb measured several observables in the decays $B^\pm \to DK^\pm$ and $B^\pm \to D\pi^\pm$, with $D \to K^0_S K^\pm\pi^\mp$. These include CP asymmetries (A) and ratios of yields (R). As with other $B^+ \to Dh^+$ decays, the process can proceed via a D^0 or $\overline{D}^0$, and the two amplitudes interfere. The nature of the interference depends on the position in the $D \to K^0_S K^\pm\pi^\mp$ Dalitz plot. The relevant properties of the D decay have been quantified in a model-independent way in previous measurements by CLEO-c in quantum-correlated D-meson decays [17]. Using these as inputs, constraints on γ (and the related quantities r_B, δ_B, r_B^π, δ_B^π) may be deduced from the A and R observables. These observables are measured at LHCb from the efficiency-corrected $B^\pm \to Dh^\pm$ yields. The fit to obtain those yields is somewhat complex: as well as splitting the sample by $B^\pm$ charge and by whether the hadron h is a pion or kaon, it is also split by same-sign ($B^\pm \to (D \to K_S K^\pm\pi^\mp)h^\pm$) vs opposite-sign ($B^\pm \to (D \to K_S K^\mp\pi^\pm)h^\pm$), by whether the point in the Dalitz plot lies within the $K^{*\pm}$ region, and by whether the K^0_S is reconstructed from long or downstream tracks. After fitting each of the subsamples simultaneously and correcting for efficiency, the set of seven CP observables (four asymmetries and three yield ratios) is measured for the each of the $K^{*\pm}$ and non-$K^{*\pm}$ regions. For the $K^{*\pm}$ region, model-independent inputs from CLEO-c are already available (and hence constraints on γ and related observables can be obtained); for the non-$K^{*\pm}$ regions, further measurements at CLEO-c or BESIII are required. The new LHCb paper uses the full Run1–2 dataset, and supersedes a previous result that used only Run1 [18].

As well as studying CKM angles, measurements of the sides of the CKM triangle are necessary to probe the overall consistency of the Standard Model. Since $\sin(2\beta)$ is particularly well known, constraining the side of the triangle opposite β, with length $|V_{ub}/V_{cb}|$, is an important part of the CKM closure test. For several years, there has been a tension between inclusive and exclusive measurements of $|V_{cb}|$. In [19], LHCb has made the first measurement of $|V_{cb}|$ with B^0_s decays, using an exclusive method with the final states $B_s^0 \to D_s^- \mu^+ \nu_\mu$ and $B_s^0 \to D_s^{*-} \mu^+ \nu_\mu$ (where the photon or π^0 in the D_s^{*-} decay is not reconstructed). This measurement is inherently complicated at a hadron collider due to the missing momentum of the neutrino (and γ/pi^0, for D_s^{*-}). On the other hand, the large boost means that the momentum direction of the B_s^0 can be inferred from its displacement vector. This is used to construct a new variable $p_\perp$, defined as the projection of the D_s^+ momentum perpendicular to the B_s^0 direction. This variable is fully and unambiguously reconstructed and is correlated with $q^2 = m^2(\mu^+\nu_\mu)$ and the related variable w. Consequently, for form factors parameterised as functions of w, it allows for templated multidimensional fits. Using such fits on the Run 1 data, $|V_{cb}|$ is measured to be $(41.4 \pm 0.6 \pm 0.9 \pm 1.2) \times 10^{-3}$ with the CLN parameterisation [20], and $(42.3 \pm 0.8 \pm 0.9 \pm 1.2) \times 10^{-3}$ with the BGL parameterisation [21]. These values are consistent with one another, and are also consistent with the world-average values of $|V_{cb}|$ from inclusive and exclusive measurements.

To date, *CP* violation has never been observed in the decay of a baryon. In [22], a search for CPV in the b-baryon decay $\Lambda_b^0 \to p\pi^-\pi^+\pi^-$ is presented using data from 2011–17. This follows on from and extends an earlier analysis of Run1 data in which evidence for CPV was found at the 3.3σ level. To search for *CP* asymmetries in the four-body phase space, the previous analysis used the method of triple-product asymmetries, measured in bins $|\Phi$, where Φ is the angle between the $p\pi^-{}_1$ and $pippim_2$ decay planes. The new analysis uses the same with an extended binning scheme (of which the previous one is a subset). In addition, it adds an unbinned search for CPV based on the energy test method. Despite a factor four increase in signal yield, the CPV significance decreases slightly: the largest values among the tests performed are 2.9σ with the triple-product method and 3.0σ with the energy-test method. The result therefore remains interesting but unconfirmed, and will require additional data to probe further.

3.2 Rare decays and lepton flavour violation

Previous results on tests of lepton flavour universality in b-meson decays have attracted interest. The observables R_K and R_{K^*}, defined as the ratio of branching fractions of $B \to X\mu^+\mu^-$ and $B \to Xe^+e^-$ for $X = K^+$ or K^{*+} and in a specified region of $q^2 = m^2(\ell^+\ell^-)$, have been measured to be below unity by around $2\frac{1}{2}\sigma$. The pattern of results is intriguing but not statistically significant: further studies are required. In [23], LHCb has extended the programme of measurements to the baryon sector, measuring the ratio of branching fractions of the decays $\Lambda_b^0 \to pK^-\ell^+\ell^-$ for $\ell = \mu, e$ in the range $0.1 < q^2 < 6.0\,\mathrm{GeV}^2$. Similarly to previous R_X studies, the measurement is carried out as a double ratio with respect to the high-rate $\Lambda_b^0 \to pK^- J/\psi$, $J/\psi \to e^+e^-, \mu^+\mu^-$ decays to minimise systematic effects, and the control measurement of the ratio of the two $\Lambda_b^0 \to pK^- J/\psi$ modes is found to be consistent with unity ($r_{J/\psi}^{-1} = 0.96 \pm 0.05$). However, unlike previous studies the lower-statistics electron yield is taken as the numerator, to produce more Gaussian

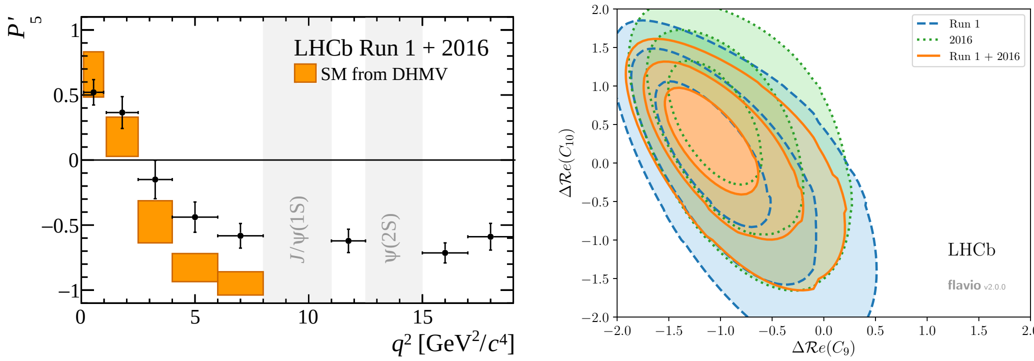

Figure 2: Left: Results for the CP-averaged angular observable P_5' measured in $B^0 \to K^{*0}\mu^+\mu^-$ in bins of q^2. The data are compared to SM predictions. Right: Results of a fit with the FLAVIO software package to the LHCb $B^0 \to K^{*0}\mu^+\mu^-$ measurements, expressed in terms of shifts in the real part of the Wilson coefficients C_9 and $C10$ relative to the SM expectation. The contour for the 2016 data alone is for illustrative purposes only and does not include full systematic uncertainties, nor coverage and bias corrections. From LHCb-PAPER-2020-002 [24].

uncertainties. The result obtained is

$$R_{pK}^{-1} = 1.17^{+0.18}_{-0.16} \pm 0.07,$$

corresponding to a central value of R_{pK} of 0.86. The result is compatible with the SM prediction of unity at the 1σ level—though it continues the trend of R_X values on the lower side of 1.

In [24], another study of $b \to s\ell^+\ell^+$ penguin decays is presented, this time an angular analysis of the process $B^0 \to K^{*0}\mu^+\mu^-$ using data from Run 1 plus 2016. This updates a previous LHCb study, in which mild tension with the SM was seen. The multidimensional phase space requires an angular analysis, performed in bins of the dimuon invariant mass squared q^2, to properly capture the physics of the decay. A number of different angular bases, with associated sets of observables, can be used; while at a mathematical level these are interchangeable, the observables can be chosen to partly cancel theory uncertainties arising from hadronic effects. The analysis reports measurements of the observables for two bases, including one with optimised observables (such as P_5'). In addition, constraints on the Wilson coefficients C_9 and C_{10} are inferred from the observables. These results are illustrated in Fig. 2. The overall level of compatibility with the SM is estimated to be 3.3σ, using current estimates of theory inputs and their uncertainties. This represents a mild increase in the tension with the SM (3.0σ to 3.3σ in a like-for-like comparison), and the pattern of small deviations seen is consistent with that expected from other lepton-flavour anomalies.

Several of the models of new physics proposed to explain the lepton-flavour anomalies, such as leptoquarks, would also imply nonconservation of charged lepton flavour quantum numbers. This could manifest as nonzero rates of processes forbidden in the SM, particularly those involving third-generation leptons. In [25], the search for such a process, $B^+ \to K^+\mu^-\tau^+$, is presented. The analysis uses most of the available data (2011–12, 2016–17). To avoid the experimental complications associated with reconstruction of a τ decay (limited branching fraction, missing momentum from neutrino(s)), the analysis uses a novel method of tagging the B^+ via a $B^{*0}_{s2} \to B^+K^-$ decay. This adds additional kinematic constraints. Thanks to these constraints, it is not necessary to fully reconstruct the τ lepton; instead, a single charged track is required for background suppression purposes. No signal is found, and upper limit of $B(B^+ \to K^+\mu^-\tau^+) < 3.9 \times 10^{-5}$ is set at the 90% confidence level.

Two searches for very rare decays that are possible but highly suppressed in the SM have been carried out. In [26], searches for the processes $B^0_{(s)} \to e^+e^-$ are performed using 2011–16 data. In the SM, they are expected to occur at rates of $\mathcal{B}(B^0_s \to e^+e^-) = 9 \times 10^{-14}$ and $\mathcal{B}(B^0 \to e^+e^-) = 2 \times 10^{-15}$, well below the current experimental sensitivity. Due to bremsstrahlung, the e^+e^- peaks would be broader than the corresponding $\mu^+\mu^-$ peaks. Consequently, it would not be possible to resolve B^0_s and B^0 peaks in the e^+e^- mass spectrum as is done for $\mu^+\mu^-$. Instead, upper limits are set using the CL_s method for each in turn, assuming an absence of the other: assuming no contribution from $B^0 \to e^+e^-$ decays, $\mathcal{B}(B^0_s \to e^+e^-) < 9.4 \times 10^{-9}$; and assuming no $B^0_s \to e^+e^-$, $\mathcal{B}(B^0 \to e^+e^-) < 2.5 \times 10^{-9}$, with both limits at the 90% confidence level. In each case, this improves on the previous limit by more than one order of magnitude.

In [27], a search for $K^0_{\mathrm{S}} \to \mu^+\mu^-$ is carried out using the 2016–18 data. The expected branching ratio in the SM is $(5.2 \pm 1.5) \times 10^{-12}$, where the theory uncertainty is dominated by long-distance effects. No evidence for a signal is found in the LHCb data, and a profile likelihood is reported as a function of the BF. In combination with a previous LHCb result based on the Run1 data, a limit of $\mathcal{B}(K^0_{\mathrm{S}} \to \mu^+\mu^- < 2.1 \times 10^{-10}$ at the 90% confidence level is set. This is the most stringent limit to date.

3.3 Decays of heavy-flavour hadrons

In [28], the first observation of the decay $B^+ \to p\bar{p}\mu^+\nu_\mu$ is reported along with a measurement of its differential branching fraction as a function of the $p\bar{p}$ invariant mass. The overall branching fraction is measured relative to the normalisation mode $B^+ \to J/\psi K^+$, and is found to be $\mathcal{B}(B^+ \to p\bar{p}\mu^+\nu_\mu) = (5.27^{+0.23}_{-0.24} \pm 0.21 \pm 0.15) \times 10^{-6}$, where the third uncertainty is associated with the normalisation BF. The differential rate reveals that the decays are strongly concentrated at low $p\bar{p}$ invariant mass, close to threshold. Such a threshold enhancement is expected from perturbative QCD predictions, and similar effects have been seen in hadronic decay channels.

In [29], LHCb presented a study of isospin-breaking effects, examining two pairs of decay modes with the full Run1–2 dataset. In each case the two modes are related but proceed through amplitudes with different isospin transitions. In the first case, $\Lambda_b^0 \to J/\psi\,\Lambda$ is compared to $\Lambda_b^0 \to J/\psi\,\Sigma^0$. Both proceed predominantly via a $b \to c\bar{c}s$ weak transition, so no change in isospin is expected. The initial state Λ_b^0 has isospin zero in the quark model, as do J/ψ and Λ, whereas Σ^0 has isospin 1. Therefore, the Λ mode leaves isospin unchanged ($\Delta I = 0$) whereas the Σ^0 mode is a $\Delta I = 1$ transition and hence strongly suppressed for $b \to c\bar{c}s$. After correcting for the difference in phase space, the amplitude ratio can be determined from the ratio of branching fraction. No significant signal for $\Lambda_b^0 \to J/\psi\,\Sigma^0$ was found, and an upper limit of (1/20.9) was placed on the amplitude ratio $|A_1/A_0|$ at the 95% confidence level. In the second case, the two modes are $\Xi_b^0 \to J/\psi\,\Xi^0$ (via $b \to c\bar{c}s$, with $\Delta I = 0$) and $\Xi_b^0 \to J/\psi\,\Lambda$ (via $b \to c\bar{c}d$, with $\Delta I = 1/2$). After removing known CKM and phase-space factors, the ratio of branching fractions of these modes is predicted to be [30,31] $1/\sqrt{6} \approx 0.41$. The decay $\Xi^0 \to \Lambda\pi^0$ is not viable at LHCb, so instead the isospin-related mode $\Xi_b^- \to J/\psi\,\Xi^-$ is used as a proxy[1]. The ratio of amplitudes measured is $|A_0/A_{1/2}| = 0.44 \pm 0.06 \pm 0.02$, fully consistent with theory expectations.

In [32], a measurement of the branching fraction of $B_s^0 \to K_S^0 K_S^0$ is reported. In the SM, the BR of this flavour-changing neutral-current process is predicted to lie in the range (15–25)$\times 10^{-6}$. The rate is measured at LHCb relative to $B^0 \to \phi K_S^0$ using data from 2011–16 and found to be $\mathcal{B}(B_s^0 \to K_S^0 K_S^0) = (8.3 \pm 1.6 \pm 0.9 \pm 0.8 \pm 0.3) \times 10^{-6}$, where the third and fourth uncertainties are associated with the normalisation mode and with f_s/f_d, respectively. This is the most precise measurement to date, and is compatible both with SM expectations and with a previous Belle measurement. This result, in a mode containing only displaced tracks, emphasises the capabilities of the LHCb detector and the flexibility of its trigger system.

3.4 Spectroscopy

In [33], new results on the quantum numbers of several excited states of the D system were published with data collected from 2011–16, using the decay process $B^- \to D^{*+}\pi^-\pi^-$ as a laboratory. With an exclusive decay process in which the initial state is fully determined, the nature of $D^{*+}\pi^-$ resonances can be probed via a four-body amplitude analysis using quasi-model-independent techniques. The resonance parameters (mass, width) and quantum numbers were measured for several states: the $D_1(2420)$, $D_1(2430)$, $D_0(2550)$, $D_1^*(2600)$, $D_2(2740)$, and $D_3^*(2750)$. Since the states $D_1(2420)$ and $D_1(2430)$ have the same external J^P quantum numbers and are close in mass, they are expected to mix; the mixing parameters were measured and the mixing angle was found to deviate from zero (no mixing) by 2.3σ.

Two new papers on beauty baryon spectroscopy were submitted. In [34], a search for Ω_b^- resonances in the $\Xi_b^0 K^-$ final state is presented, with two first

[1] It may seem curious to assume isospin in order to test isospin, but we are testing the null hypothesis here.

Table 2: Summary of the peak parameters of the four $\varXi_b^0 K^-$ peaks in [34], showing the peak positions of $\delta M = M(\Xi_b^0 K^-) - M(\Xi_b^0)$, the masses, and 90% (and 95%) confidence level upper limits on the natural widths. The indicated uncertainties are statistical, systematic, and due to the world-average value of the $\varXi_b^0$ mass (for the masses). For the $\varOmega_b^-(6350)^-$ peak, the central value of the width is also indicated.

Peak	Mass [MeV]	Width [MeV]	Significances [σ]	
$\varOmega_b^-(6316)^-$	$6315.64 \pm 0.31 \pm 0.07 \pm 0.50$	< 2.8 (4.2)	3.6	2.1
$\varOmega_b^-(6330)^-$	$6330.30 \pm 0.28 \pm 0.07 \pm 0.50$	< 3.1 (4.7)	3.7	2.6
$\varOmega_b^-(6340)^-$	$6339.71 \pm 0.26 \pm 0.05 \pm 0.50$	< 1.5 (1.8)	7.2	6.7
$\varOmega_b^-(6350)^-$	$6349.88 \pm 0.35 \pm 0.05 \pm 0.50$	$\begin{cases} < 2.8\ (3.2) \\ 1.4\,^{+\,1.0}_{-\,0.8} \pm 0.1 \end{cases}$	7.0	6.2

observations of new states plus hints of two more (see Fig. 3). All four peaks are narrow, with widths below 3.1 MeV at the 90% confidence level. The fitted parameters and the significances of the peaks are given in Table 2. While the states cannot be positively identified with the data available, they appear consistent with the simplest explanation, namely that these are low-lying $L = 1$ excitations. The pattern of the peaks is qualitatively similar to that of the $\varOmega_c^0 \to \varXi_c^+ K^-$ resonances observed in a previous LHCb paper [35]; since there is a close analogy between the c-baryon and b-baryon systems, the $\varXi_b^0 K^-$ spectrum can provide a useful testing ground for models previously applied to the $\varXi_c^+ K^-$ final state.

In the second paper, Ref. [36], an analysis of the $\varLambda_b^0 \pi^+\pi^-$ was presented. This final state has been studied before at LHCb: in one of our earliest spectroscopy papers from 2012 [37], two narrow states were observed close to threshold, the $\varLambda_b(5912)^0$ and $\varLambda_b(5920)^0$; and in a more recent paper from 2019 [38] the presence of two further narrow resonances at higher mass and very close to one another, the $\varLambda_b(6146)^0$ and $\varLambda_b(6152)^0$, was observed. In the new analysis, the near-threshold states are remeasured with improved precision and the intermediate region 5950–6130 MeV is explored. A broad structure is present, but to study it with precision the analysis uses an improved selection (including a multivariate selector and, to study the region away from threshold, a cut of 250 MeV on the p_T of the dipion system). The analysis also uses two different $\varLambda_b^0$ decay modes (to $\varLambda_c^+\pi^+$ and $J/\psi\, pK^-$), both to increase the available statistics and to provide a further cross-check; the inclusive $\varLambda_b^0$ yields are approximately 938k and 223k for the two channels. Separate fits are carried out in the near-threshold regions (to study the $\varLambda_b(5912)^0$ and $\varLambda_b(5920)^0$) and in the broader region $5930 < m(\varLambda_b^0\pi^+\pi^-) < 6230$ MeV. In each case, a simultaneous fit to six mass spectra is used (the two $\varLambda_b^0$ decay modes, for each of $\varLambda_b^0\pi^+\pi^-$, $\varLambda_b^0\pi^+\pi^+$, $\varLambda_b^0\pi^-\pi^-$, with the latter two wrong-charge modes used to control the background). The broad structure is observed with high significance, in excess of 14σ and 7σ in the two final states. Due to its large width, the variation in phase space $\rho_3(m)$ across the resonance must be taken into account.

It is fitted with the following lineshape:

$$f(m|m_0,\Gamma) \propto \frac{\Gamma\rho_3(m)}{\left(m_0^2-m^2\right)^2+m_0^2\,\Gamma^2\left(\frac{\rho_3(m)}{\rho_3(m_0)}\right)^2}.$$

Its mass and width are measured to be:

$$\begin{aligned} m &= 6072.3\pm 2.9\pm 0.6\pm 0.2\,\mathrm{MeV}/c^2, \\ \Gamma &= 72\pm 11\pm 2\,\mathrm{MeV}, \end{aligned}$$

where the third uncertainty arises from the $\mathit{\Lambda}_b^0$ mass. The new state is consistent with the first radial excitation of the Λ_b^0 baryon, the $\Lambda_b(2S)^0$ resonance. The mass and width of the $\mathit{\Lambda}_b(5912)^0$ and $\mathit{\Lambda}_b(5920)^0$ are also measured, with significantly improved precision compared to the previous result.

Three new results on the spectroscopy and properties of $\mathit{\Xi}_{cc}$ baryons have also been submitted. Two concern the properties of the $\mathit{\Xi}_{cc}^{++}$ state discovered by LHCb in 2017, and the third is a search for its isospin partner state, $\mathit{\Xi}_{cc}^{+}$, which has yet to be observed[2]. In [39], the production cross-section of the $\mathit{\Xi}_{cc}^{++}$ was investigated using the 2016 data, with $\mathit{\Xi}_{cc}^{++}\to\mathit{\Lambda}_c^+K^-\pi^+\pi^+$ and $\mathit{\Lambda}_c^+\to pK^-\pi^+$. This requires careful treatment of the data to properly control the L0 (hardware) trigger efficiency. Two disjoint subsamples of data are used: one in which L0 is fired by one or more of the decay products of the $\mathit{\Lambda}_c^+$ (TOS), and another in which L0 is fired by other activity in the event *and* not by the $\mathit{\Lambda}_c^+$ decay products (exTIS). In both cases, the cross-section is measured relative to that of promptly produced $\mathit{\Lambda}_c^+$. For TOS, the trigger channel is the same for signal and normalisation modes, helping to reduce systematic uncertainties; for exTIS, the estimated trigger efficiency is compared to that of B_c^+, another doubly heavy state. The cross-sections measured in the two subsamples are fully consistent with one another. For an assumed $\mathit{\Xi}_{cc}^{++}$ lifetime of 256 fs, $\sigma(\mathit{\Xi}_{cc}^{++})\mathcal{B}(\mathit{\Xi}_{cc}^{++}\to\mathit{\Lambda}_c^+K^-\pi^+\pi^+)/\sigma(\mathit{\Lambda}_c^+) = (2.22\pm 0.27\pm 0.29)\times 10^{-4}$.

Secondly, in [40] a measurement of the $\mathit{\Xi}_{cc}^{++}$ mass was performed using all of the Run 2 data sample with suitable triggers: 2016–18. Both of the previously observed decay modes, $\mathit{\Xi}_{cc}^{++}\to\mathit{\Lambda}_c^+K^-\pi^+\pi^+$ and $\mathit{\Xi}_{cc}^{++}\to\mathit{\Xi}_c^+\pi^+$ were used. Improving on previous studies that used only the 2016 data, the mass was measured to be $3621.55\pm 0.23(\mathrm{stat})\pm 0.30(\mathrm{syst})\,\mathrm{MeV}/c^2$. It is worth pausing to note that less than three years after the initial discovery, we are now working with a yield of around 2200 events and are systematically limited in precision on the mass. The dominant systematic uncertainties arise from the momentum-scale calibration and from the input values of the $\mathit{\Lambda}_c^+$ and $\mathit{\Xi}_c^+$ masses. Further improvements in precision will require the addition of more decay modes with lower energy release (and therefore likely smaller branching fractions).

[2]The state reported by SELEX, being 100 MeV/c^2 lower in mass, cannot be the isospin partner of the $\mathit{\Xi}_{cc}^{++}$.

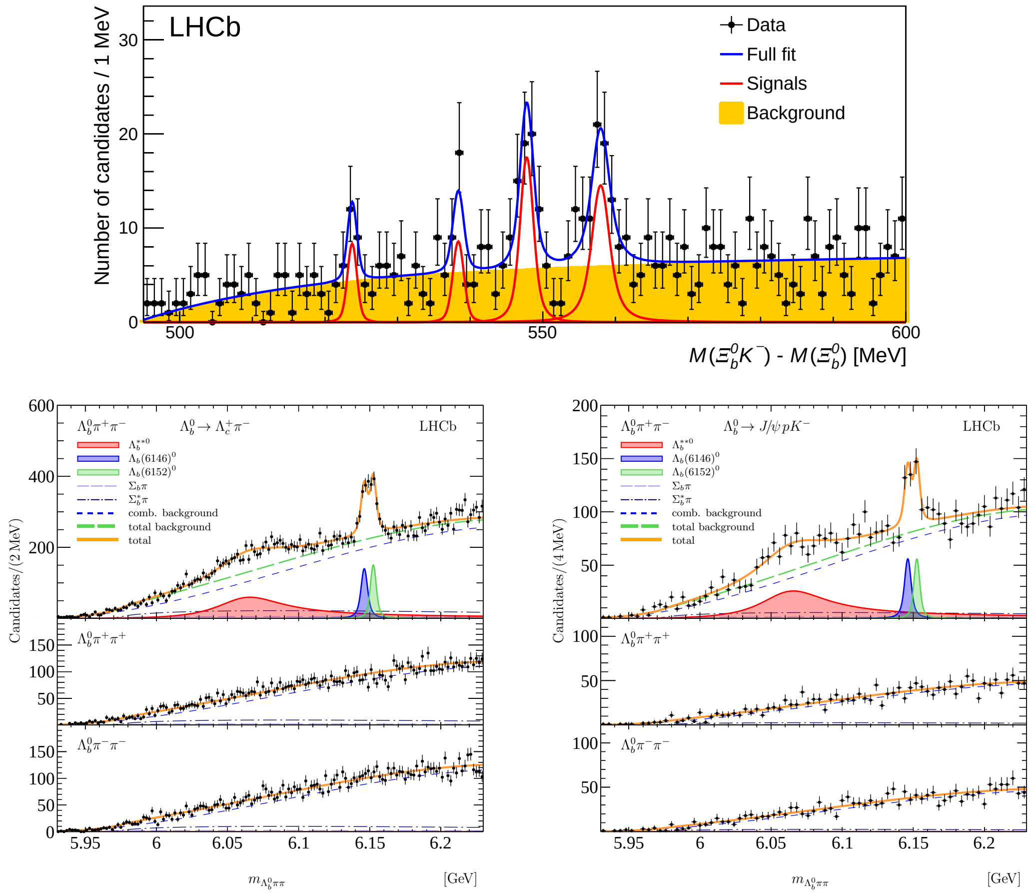

Figure 3: Upper: Distribution of the mass difference for $\Xi_b^0 K^-$ candidates, showing four peaks (of which two exceed the observation threshold). Lower: Mass spectra $\Lambda_b^0\pi\pi$, for (left) $\Lambda_b^0 \to \Lambda_c^+\pi^+$, (right) $\Lambda_b^0 \to J/\psi pK^-$. From LHCb-PAPER-2019-042 [34] and LHCb-PAPER-2019-045 [36].

Thirdly, in [41] a search for the singly charged Ξ_{cc}^+ (ccd) state was presented, using the full LHCb dataset and the final state $\Lambda_c^+K^-\pi^+$. This updates a previous LHCb search that used only the 2011 data. A wide mass range of 3400–3800 MeV/c^2 was used for the search, chosen to include both the SELEX and LHCb reported mass values for Ξ_{cc} states. The analysis was carried out blind, using two different signal selections: the first optimised for sensitivity to the presence of a Ξ_{cc}^+ signal, and the second optimised for setting limits on the Ξ_{cc}^+ cross-section relative to the Ξ_{cc}^{++} and Λ_c^+ (and which therefore required cuts to be aligned between the decay modes; the L0 trigger requirement discussed above is a good example of this). No statistically significant excess was found. The largest local excess, at a mass of around 3620 MeV/c^2, had a local significance of 2.7σ when taking account of systematic uncertaintes, and a global significance of 1.7σ. The mass at which this excess occurs is suggestive, and lends hope that future updates with new decay modes in the Run1–2 data, or with the first half of the Run3 data, will finally pin down the state.

3.5 QCD physics and production

Measurements of production rates and asymmetries are useful inputs for tuning models that describe the proton-proton collision, and serve an important purpose in improving the simulations used at all LHC experiments. In addition to this broad goal, certain measurements are also needed as direct inputs to other studies—for example, results reported above require knowledge of f_s/f_d. Since the last RRB report, LHCb has made three measurements of production properties in addition to the Ξ_{cc}^{++} production rate discussed in the preceding section.

In [42], the variation of f_s/f_d with the pp collision energy is studied using $B_s^0 \to J/\psi\,\phi$ and $B^+ \to J/\psi\,K^+$ decays. Data at $\sqrt{s} = 7$, 8, 13 TeV are analysed and compared in bins of $p(B)$, $p_z(B)$, $p_{\mathrm{T}}(B)$, $\eta(B)$, and $y(B)$. Of these, the ratio f_s/f_d is found to show significant variation only with $p_{\mathrm{T}}(B)$. Evidence (4.8σ) is also found that f_s/f_d increases with $\sqrt{s}$.

A measurement of the production fraction of B_c^+ mesons, $f_c/(f_u + f_d)$, is reported in [43], using the exclusive semileptonic decay $B_c^- \to J/\psi\,\mu^-\bar{\nu}_\mu$ and the inclusive semileptonic decays $B \to D^0 X\mu^-\bar{\nu}_\mu$ and $B \to D^+ X\mu^-\bar{\nu}_\mu$. In previous, related measurements of B_s^0 and Λ_b^0 production, the method relies on semileptonic decays being dominated by a single tree diagrams in which the light quark(s) may be treated as spectators, implying that the semileptonic widths of B^+, B^0, B_s^0, Λ_b^0, Ξ_b, *etc.* are equal to a good approximation. However, for B_c^+ this approach is not possible due to the presence of two heavy quarks. Instead, a value of $\mathcal{B}(B_c^- \to J/\psi\,\mu^-\bar{\nu}_\mu)$ is taken from theory predictions, and this is in turn used to obtain $f_c(7\,\mathrm{TeV}) = (2.58 \pm 0.05 \pm 0.62 \pm 0.09) \times 10^{-3}$ and $f_c(13\,\mathrm{TeV}) = (2.61 \pm 0.03 \pm 0.62 \pm 0.06) \times 10^{-3}$, where the second uncertainty is systematic and includes the assumed value of $\mathcal{B}(B_c^- \to J/\psi\,\mu^-\bar{\nu}_\mu)$, and the third is due to input values of B_s^0 and Λ_b^0 production fractions. Finally, the B_c^+ production asymmetry is also measured, and is found to be fully consistent with zero: values of $(-2.5 \pm 2.1 \pm 0.5)\%$ and $(-0.5 \pm 1.1 \pm 0.4)\%$ are obtained for $\sqrt{s} = 7$, 13 TeV, respectively.

In [44], the production of $\eta_c(1S)$ mesons at $\sqrt{s} = 13$ TeV is studied using the decay mode $\eta_c(1S) \to p\bar{p}$. The $\eta_c(1S)$ can be produced promptly at the primary vertex or in the decays of b hadrons (secondary production). As in previous analyses of charmonium production, the two components are separated using the pseudo-proper-decay-time $t_z = \Delta z\, m/p_z$, where Δz is the z component of the vector between the reconstructed $\eta_c(1S)$ decay vertex from the PV, p_z is the z component of the $\eta_c(1S)$ momentum, and m is the reconstructed $\eta_c(1S)$ mass. For the prompt case, $\eta_c(1S)$ and J/ψ signals are visible above an extremely large background; for the secondary case, the background is much reduced by a vertex separation requirement, so despite lower yields the S/B is higher. The overall prompt and secondary $\eta_c(1S)$ cross-sections are measured (in the kinematic range

$6.5 < p_{\mathrm{T}} < 14$/gevc and $2.0 < y < 4.5$) relative to J/ψ. Singly differential measurements are also made in bins of p_{T}. Overall, prompt $\eta_c(1S)$ production is found to be $\sigma_{\eta_c(1S)} = 1.26 \pm 0.11 \pm 0.08 \pm 0.14\,\mu\mathrm{b}$, where the third uncertainty is associated with the J/ψ normalisation mode. Secondary production of $\eta_c(1S)$ relative to J/ψ is found to be $\mathcal{B}_{b\to\eta_c X}/\mathcal{B}_{b\to J/\psi X} = 0.48 \pm 0.03 \pm 0.03 \pm 0.05$, where the third uncertainty is associated with branching fraction inputs. Finally, the clean, high-statistics sample of secondary $\eta_c(1S)$ and J/ψ decays are used to measure the mass difference between the two states to be $m(J/\psi) - m(\eta_c(1S)) = 113.0 \pm 0.7 \pm 0.1\,\mathrm{MeV}/c^2$; this is the most precise single measurement to date.

3.6 Heavy-ion physics

LHCb has released three conference notes related to heavy-ion and high-multiplicity physics recently. Two of these concern proton-lead collision data, taken with $\sqrt{s_{\mathrm{NN}}} = 8.16\mathrm{TeV}$ in 2016. These correspond to an integrated luminosity of $12.2\,\mathrm{nb}^{-1}$ in the forward (pPb) configuration plus $18.6\,\mathrm{nb}^{-1}$ in the backward (Pbp) configuration. In [45], measurements of the Z production cross-section are presented, with $\sigma(Z \to \mu^+\mu^-, p\mathrm{Pb}) = 28.5\pm1.7\pm1.2\pm0.7\,\mathrm{nb}$ and $\sigma(Z \to \mu^+\mu^-, \mathrm{Pb}p) = 13.4\pm1.0\pm1.4\pm0.3\,\mathrm{nb}$, where the third uncertainty is associated with the integrated luminosity. In [46], prompt charm production is studied in the same environment. Summing over D^0 and $\overline{D}^0$, the integrated cross-section in $0 < p_{\mathrm{T}} < 16\,\mathrm{GeV}/c$ is found to be $288.3 \pm 0.2 \pm 17.4\,\mathrm{mb}$ in the forward rapidity range $1.5 < y^* < 4$ and $308.9 \pm 0.1 \pm 30.5\,\mathrm{mb}$ in the backward range $-5 < y^* < -2.5$.

In [47], the methods of heavy-ion physics are applied to spectroscopy in pp data, studying the relative production rates of $\chi_{c1}(3872)$ (the state formerly known as $X(3872)$) and $\psi(2S)$ as a function of event multiplicity. As used in the $\eta_c(1S)$ measurement discussed in the previous section, the pseudo-proper-decay-time t_z is used to separate prompt from secondary production. This is important here since promptly produced charmonia will be exposed to the pp collision environment, whereas those originating at a b-hadron decay vertex several mm away will not: thus, prompt production as a function of multiplicity probes differences between the structure of the $\chi_{c1}(3872)$ and $\psi(2S)$, whereas secondary production acts as a control and should be flat[3]. Using data from 2012, hints of a multiplicity dependence (at the 2.6σ level) are seen in prompt production. Such an effect might arise if the $\chi_{c1}(3872)$ is a weakly bound state, such as a $D^0\overline{D}^{*0}$ hadronic molecule. Further analysis with more statistics will be required to determine if the effect is significant.

3.7 Exotica and BSM searches

In [48], a search for dark photons ($A' \to \mu^+\mu^-$) in the 2016–18 data is presented. The search covers both candidates that decay promptly and those with a longer

[3] b-hadron production might be affected by the pp environment and multiplicity, but this will cancel in the ratio between secondary $\chi_{c1}(3872)$ and secondary $\psi(2S)$.

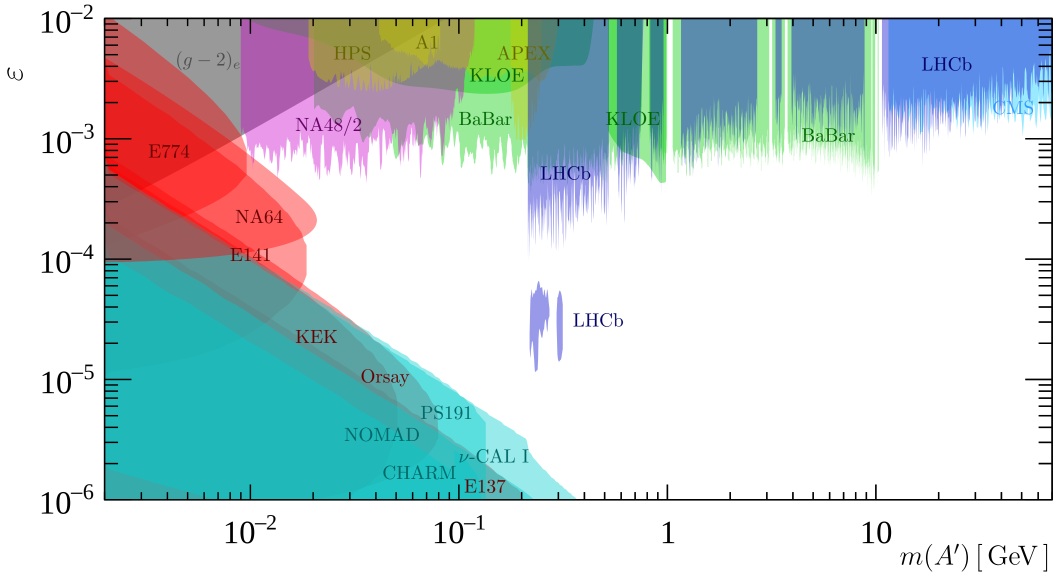

Figure 4: Comparison of the LHCb results on dark photons to existing constraints from previous experiments in the few-loop ε region From LHCb-PAPER-2019-031 [48].

lifetime. In both cases, the constraints may be expressed as excluded regions in the $(\varepsilon, m(A'))$ plane, where ε expresses the suppression of the dark photon coupling relative to that of the SM photon. The excluded regions are illustrated in Fig. 4. The two "islands" in the centre of the plot correspond to the search for longer-lived dark photons, which would have smaller values of ε. With data from the LHCb upgrade, the exclusion region is expected to expand significantly.

4 Status of upgrade: tracking system

Over the last six months the tracking system has made considerable progress. The Vertex Locator (VELO) has started module serial production, finished the production of two pairs of RF boxes (one pair etched to 150 μm, ready for installation, and one kept as spare) and the construction of mechanical structures is almost complete. The Upstream Tracker (UT) has started module production. Four-chip hybrids have been produced in large quantities and first panels populated with SALT v3.5 chips. One wafer of the 3.8 SALT version has been produced and tested. First results on a four-chip hybrid are encouraging. The 8-chip hybrid is currently being designed. The first few instrumented staves are being produced. The large Scintillating-Fibre (SciFi) Tracker is being assembled at CERN, in the surface building. Construction of the first six C-frames (one half of the detector) is well under way. A more detailed summary of recent progress and plans for the next half year are given for each of the three sub-detectors of the tracking system.

4.1 Vertex Locator (VELO)

4.1.1 Module Components

Each of the 52 VELO modules is equipped with four sensor-ASIC pixel hybrid triplets (two per side), associated with four front-end hybrids, two GBTX hybrids, and corresponding power and data cables, as well as the so-called "interconnect" cables which route signals between the hybrids. The triplet electrical testing has been completed for all production triplets with the exception of the IV curves which will be completed on the last 25% of the production batch within a month. The production quality issues on the front-end hybrids were successfully addressed with the switch to the new vendor. The hybrids are now only accepted after a detailed visual inspection at CERN, and enough hybrids are already in hand to complete the production. All GBTX hybrids have been manufactured, and following the issues discovered during the production and assembly a systematic thermal cycling check to $-35°C$ was added to the standard electrical and visual check. This QA is complete and the hybrids are fully in hand. The interconnect cables were produced with residual manufacturing issues, which can be resolved with visual inspection and re-soldering of the connectors where necessary. The re-soldering is done, and the visual inspection will be completed for full production within two months. The High speed data tapes and the long HV cables have been fully produced, have had the connectors mounted, and have undergone a long programme of exhaustive visual checks and electrical testing, including full impedance measurements. The six different categories (varied by parity and length) are now all fully produced, tested and delivered to the assembly site.

The microchannel substrate production is complete, as previously reported, with an excellent yield from Lot 2 and the additional Lot 3. The production focus has been on the soldering attachment of the inlet/outlet pipes and connector manifold to the silicon substrate. The voidless fluxless soldering procedure is very sensitive to the quality of the pre-tinning step of the connectors, which is itself dependent on the surface quality and burr-free preparation of these connectors. The connectors have undergone numerous quality checks, with re-machining, burr removal, chemical cleaning and polishing where necessary, and the full production is expected to be completed in the next six weeks. The production has followed the need for mechanical and non-installation quality pieces at the assembly sites, and to date a total of 57 complete cooler soldering processes have been successfully achieved, with no cooler lost due to handling error. Of these there are currently in hand 19 installation quality soldered pieces, and the process is well debugged, with timely delivery to the module production sites. All other mechanical pieces for the modules, including the cable harnesses which support the power cables and route signals through a PCB, the carbon fibre legs, the invar feet, and the thermal hurdles are fully produced and have undergone QA.

4.1.2 Module Construction

The module construction procedures have been fully reviewed and 6 production and one test module (with a different glue composition) were successfully produced by the end of September. A problem then arose with the production during the thermal tests, indicating a failing thermally conducting glue joint between the silicon tile and silicon cooling substrate on one of the modules. This was manifested through a large thermal gradient on the module when testing in vacuum which was of sufficient concern to warrant further investigation. It transpired that it was possible to physically remove the tile from the substrate, and the module construction project was completely stopped while the issue was investigated. All the gluing procedures were inspected in great detail, a DCB (double cantilever bar) test stand was set up to investigate peel force resistance, and a mechanism was put in place in three different institutes to check accelerated ageing and thermal cycling. In addition to examining the previously used glue, three additional glues were investigated (plus one which was discarded at an early stage) in parallel, to guarantee that a solution could be found. One of these had not been previously fully checked for radiation resistance, and this was added to the qualification schedule. The exercise of modifying jigs and procedures to build a production quality module with an alternative glue was also fully completed. The gluing procedure was exhaustively overhauled, and it was found that improvements could be made in various areas, including protecting against the absorption of humidity by the catalyst by drying the surfaces just before attachment. The investigation has now ended and this has allowed the VELO group to move forward with complete confidence with the finally selected glue, which is Stycast 2850FT (which had been previously used) with a new catalyst, 23LV. The assembly sites are now ramping back up to full production speed, with the aim of reaching 3.5 modules per week total within four weeks.

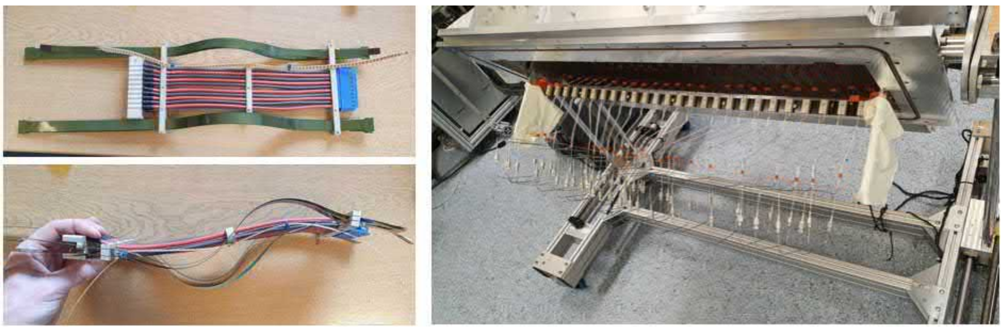

Figure 5: Cabling and piping for the VELO halves. On the left, the flexible cable looms for data, power and temperature control, which absorb the VELO motion. On the right, the network of 26 custom bent capillaries which supply the cooling CO_2.

4.1.3 Readout Chain

The Vacuum Feedthrough flanges (VFBs) have been fully and successfully produced. This very large scale project has included PCB production, component mounting, attachment of power, data, control and temperature monitoring cables, attachment of cable constraints, installation into the vacuum flange with the dedicated half moon double glue process, and final helium leak checking. There are a total of 10 flanges, and these have all been successfully produced and shipped to the assembly site. The six OPB prototype boards produced up to now have been in constant use at the module assembly sites and at the electrical readout chain test sites. Minor bug fixes and improvements have been implemented, communicated to the company, and the final production is underway. The new mechanical air cooling design has been successfully integrated.

4.1.4 Mechanics and RF Foil

The preparations for the mechanical assembly of the modules onto the bases is proceeding. The valve assemblies for the isolation vacuum and cooling manifolds have been fully delivered and characterised. The A and C side bases have been delivered and the metrology performed. The C side hood has undergone metrology and has been installed into the completed trolley, equipped with blank flanges, and vacuum checked. The LUCASZ full power cooling plant has been successfully installed, commissioned, and run with heat loads. The focus is now on the installation of the pipe runs, which has been completed and is now at the quality check stage, and the installation of the VFBs together with the cable "looms" (this refers to the cable bundle together with constraints which supplies each module and also absorbs the VELO motion). The cabling and cooling module services for one half are shown in Figure 5. This will be followed by a cooling commissioning period using temporarily mounted pre-production modules, followed by the production module mounting. By mid-June approximately half the modules will be mounted on one side, and a full scale multi-module readout test will be performed, exercising and stress testing as far as possible the electrical readout chain and cooling performance. The installation of the first VELO half is currently programmed for the second half of August.

The RF foil project has made very good progress and is now days away from completion. Following the decision to perform internal chemical etching of the installation boxes, this procedure was carried out on two of the four produced boxes, with the choice optimised following the fine grained metrology carried out at the foil production site. The final achieved thickness of the thinned face of the foils was approximately 150 μm. The two remaining installation quality boxes with a nominal 250 μm thickness are kept as spares. The boxes were shipped back to Nikhef for final metrology and leak tightness checks and were torlon coated on the inside in a specially developed process consisting of the application of 30 ultra-thin coats. After attachment of the PT100 sensors to the insides of the foil they were shipped back to CERN for NEG coating. In a final complication, it was discovered that in order to have full confidence in the NEG coating, the shiny foil surfaces should have the outermost few microns removed to relieve machining stress. This was achieved with an acid etch procedure which was developed and tested on the pathfinder foil before being applied to the installation foils. Finally the foils were transported to the LHCb experiment and pre-installed onto the detector supports ready for insertion into the VELO vacuum tank. This last step, which will be followed by the metrology and the SMOG2 integration, will take a few days and will be performed when the schedule allows. A preparatory integration of the SMOG2 has already been successfully performed for alignment purposes (see figure 14 in SMOG2 section 6).

4.1.5 Commissioning

The electrical readout chain has been fully assembled for a full module and this slice test is being upgraded to a two module setup. This includes the OPB (Opto Power Board), vacuum feedthrough, data tapes, low voltage cables, control and VeloPix hybrids and sensor triples. The set up is now being used to develop the control panels and testing procedures for the final modules. The NTC readout is being integrated together with the software interlock, and the PT100 readout board will be used as an interlock in the slice test and also at the assembly site. An end-to-end threshold scan procedure is being developed to test the readout and DAQ control, analysis framework, and develop the calibration procedures. The commissioning is happening in parallel with the VELO construction, such that commissioning at Point 8 can happen as soon as the first detector half is installed.

4.2 Upstream Tracker (UT)

All the components necessary to assemble instrumented staves are currently in advanced stage of production, with the exception of the 8-chip hybrids needed for the innermost portion of the detector, as the first prototype did not meet specifications. Note that it was implemented in FR4 technology, with a stack-up very different than the one planned for the final design. This item defines the critical path in the UT project. The boards necessary to read out and power the hybrids are in advanced stage of production and significant advances are achieved in the preparation for assembly and commissioning. A problem uncovered in the CO_2 cooling system, involving contamination with silicon oil, is being addressed and a solution has been found that is likely not to have a major impact on the construction schedule. A concern is the impact of the corona-virus related measures, especially in Italy, on the hybrid production schedule. Other aspects of the project may be impacted if similar restrictions to laboratory access or transport of components are enacted.

4.2.1 Instrumented staves

The sensor production was completed in November 2019, and all the sensors needed are available for module construction.

The 4-chip hybrid production, after some difficulties, was about to reach the target processing rate when the escalation of work restrictions due to the coronavirus started. The current status is that 80 hybrids of detector-grade quality to be installed in the detector are available at the construction site and the production and testing of more than 80 hybrid per week was commissioned when the laboratory was closed because of the coronavirus outbreak. The production can ramp up to 160 hybrids per week once the laboratory is back to operation.

The implementation of the 8-chip hybrid circuit features two major differences with respect to the 4-chip version: space limitations require the ASICs to be much closer and thus the analog power is provided from the "back" of the chip, farther from the preamplifier. The power distribution network has been refined in this version of the chip, and its good performance is illustrated in Fig. 6, where the SALT v3.8 is mounted on a 4-chip hybrid and wire-bonded to a B-type sensor (the one producing the highest input capacitance seen at the preamplifier input). Unfortunately this performance has not been replicated in the first prototype of the 8-chip hybrid. A new design is currently being reviewed and several improvements have been added. We hope to complete this process at the end of the month.

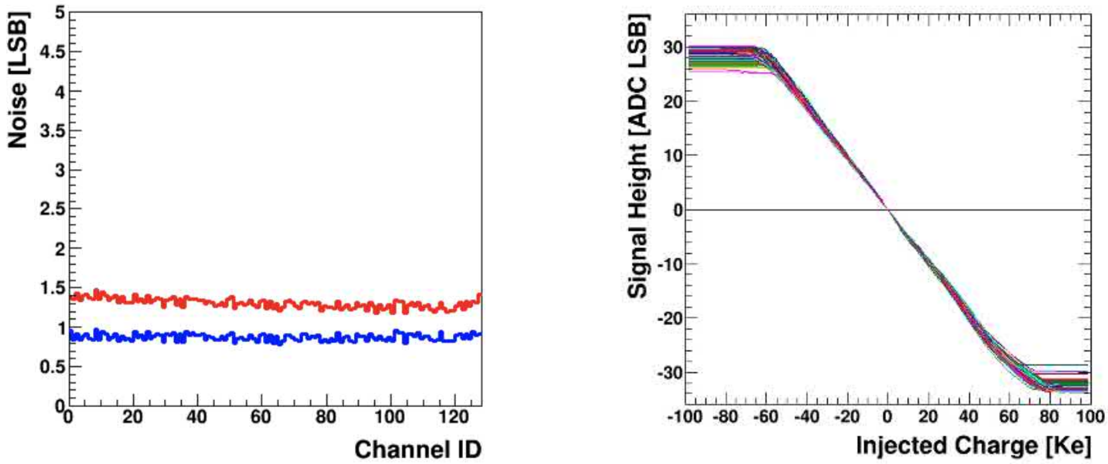

Figure 6: Electronics response measured on 4-SALT hybrid wire-bonded to type B sensor using SALT v3.8 with analog power provided from the back-bonds: (left) the noise on versus channel number, the blue line shows the common-mode subtracted noise and the red shows the total noise versus channel number, (right) gain plot with ADC sampling tuned to be close to the SALT v3.8 peaking time.

The UT module construction involves several delicate steps: hybrid detachment from the panel, gluing of hybrid and sensor on the stiffener, wire-bonding sensor and ASICs and sylgard potting of the wire bonds. In addition, the electronics is tested and high voltage is applied to the sensor at various steps in this process to assess the component integrity. The various steps in this production flow have gone through an initial refinement stage when module production has been slow and has encountered a couple of set-backs, but the production is ramping up to the final goal of assembling and testing 16 modules per day.

The modules are mounted on staves where four flex-circuits are glued. The flex-circuit provides data communication with the data control boards (DCB) and brings low-voltage and high-voltage to the hybrids. Their construction is well advanced, it is expected to end in mid-April. The majority of the articles is received at the stave construction site and the process of gluing flex-circuits onto bare staves is progressing smoothly.

The process of module attachment to staves was started in early fall with the available hybrids. The procedure went smoothly, but was paused by the lack of modules. It has recently restarted and we expect the first five staves to be completed in mid-April. As soon as the 8-chip hybrids are available we will construct some of the innermost stave to facilitate installation of the staves into their final support structure. This process, in absence of significant delays induced by corona-virus motivated restrictions, is expected to start in early June.

4.2.2 Near-detector electronics

Data from the front-end electronics and commands from the DAQ system are processed by the so called PEPI electronics comprising data control boards (DCBs) plugged in complex backplanes providing mapping from the DAQ boards (TELL40) and the SALT ASICs. In addition the backplanes distribute low voltage from regulator boards located in service bay crates in the experimental hall. These components are in advanced state of production, for example the first six backplanes have been shipped to CERN and PEPI integration will start in early April. The construction team is finalizing the burn-in procedure for the many components involved, and the target delivery time for the first half of the components is expected by early June.

4.2.3 Mechanic infrastructure and cooling and cooling

Components for the frame, box, chariot and associated mechanical infrastructure have been designed and are currently being produced. Similarly, the components needed for the CO_2 distribution system are being acquired. Some components, for example parts needed for the CO_2 manifold, have been produced. The completion of the parts needed is expected in June. A major concern was the impact of the silicon oil contamination found in the Mauve plant and in all the associated systems, but a cleaning procedure has been identified and is being implemented.

4.2.4 Integration in the experiment

The UT detector is divided into two sub-assemblies on both sides of the beam pipe. The original plan was to complete the first 1/2 (the so called C-side, captured by the beam pipe) first, but the delay in manufacturing the 8-chip hybrid led us to develop a re-optimized schedule, which aims at a completion time by the end of the year, and anticipates transitioning to side A construction with the available instrumented staves if the innermost ones are delayed. Instrumented staves will be shipped to CERN in groups of 5. The first shipment is anticipated in mid-April. In parallel the various components of the electronics infrastructure (cables, ancillary boards, patch-panels, optical fibers) are being acquired and customized for installation.

In November 2019 a type-A stave instrumented with 7 modules (one full face) has been shipped to CERN. Fig. 7 shows the instrumented stave mount in the prototype UT box. Many tests have been performed, including several thermal cycles and the performance is found to be very stable, with a powering and readout scheme that is essentially the same as in the final detector. Some valuable lessons have been learned that will make the mechanical support and mounting procedure of the various components more reliable. The hybrid performance is consistent with test-bench studies on individual modules. This stave is also an essential tool to develop and validate the monitoring and control software needed to operate the detector.

Figure 7: First instrumented stave mounted in the test box located in the assembly laboratory at point 8.

4.3 Scintillating-Fibre Tracker (SciFi)

The technology and the full detector design of the SciFi system is described in the LHCb Tracker Upgrade TDR [5]. The SciFi will consist of 250 μm thick and 2.5 m long scintillating fibres arranged as hexagonally close-packed six-layer mats of 135 mm width. Eight of these mats are joined together to form 5 m long and 52 cm wide modules. The fibres will be read out by 128-channel arrays of Silicon Photo-multipliers (SiPMs), which have to be operated at $-40°$C to limit the dark count rate after irradiation. The readout electronics is based on a custom-designed ASIC followed by digital boards for further data-processing and the optical data-transmission. The modules including the readout electronics will be mounted on support frames and will be arranged in 12 stereo layers.

4.3.1 Mat, module and SiPM production

The serial production of the fibre mats, the module production and the production of the SiPM and flex-cables have been finished in 2019.

4.3.2 Electronics and read-out box production

The readout ASIC (PACIFIC) has been produced, packaged and tested. The production of all PACIFC carrier boards and cluster boards has been concluded in the course of 2019. The last master boards have arrived from the industrial producer in January 2020. The front-end boards are mounted on cooling frames and form the so called readout-box (ROB). After an in house (Clermont-Ferrand) pre-production of 24 assemblies the remaining ROBs were assembled by an industrial producer. The last batch has arrived at CERN in week 10. Figure 8 shows a finished ROB. The ROBs are currently being tested at CERN. The quality of the assemblies is high and no major problem has been found so far. At the detector,

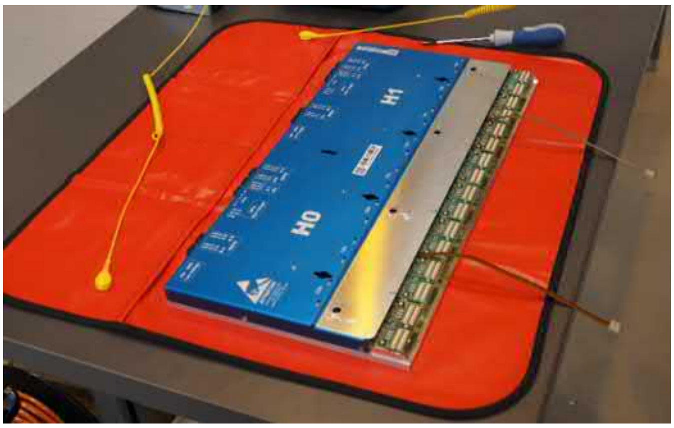

Figure 8: Photograph of a finished readout box (ROB) containing 8 PACIFC carrier boards, 8 cluster boards and 2 master boards

the ROBs are mounted on water-cooled aluminium blocks to ensure the cooling of the electronics. The aluminium-blocks and also the water-pipes are integrated into the C-frame structure. All water-cooling components, blocks and pipes, for the full detector have already been produced.

4.3.3 Cold-box

The SiPMs are not part of the readout boxes but are mounted in a separate mechanical unit, the so-called cold-box. The SiPMs are carried by a cold-bar which will be cooled down to $-40°C$ using Novec, a modern cooling liquid with minimal environmental impact. The cold-bar further allows the precise mechanical positioning of the SiPMs on the ends of the fibre modules. Sufficient thermal insulation and gas-tightness to avoid ice building is provided by the cold-box enclosure. The mass production of the cold-boxes has been completed; 90% have been shipped to CERN, the remaining ones have issues with gas tightness and are being repaired at Nikhef.

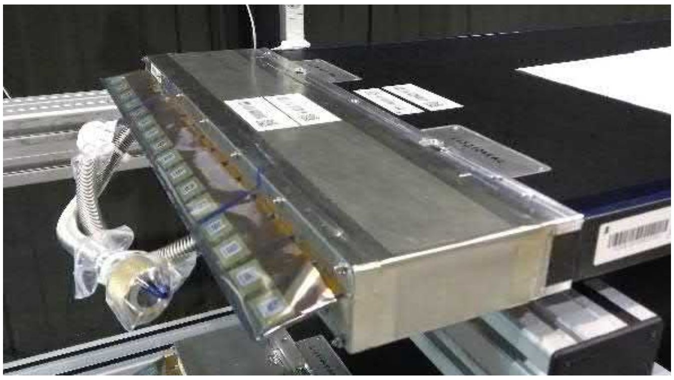

Figure 9: Photograph of a finished module with mounted cold-box. The two vacuum insulated Novec connections and the 16 SiPM flex cables are visible.

The cold-boxes are mounted on both ends of the fibre modules before installation. The flex-cables of the SiPMs will later be connected to the front-end electronics. The module finishing, i.e. the mounting of the cold-boxes onto the modules, is progressing well. Three quarters of the detector modules have already been equipped with cold-boxes. Fig. 9 shows a finished module with a mounted cold-box.

4.3.4 Mechanical structure, services, detector assembly and commissioning

Groups of five or six detector modules and their corresponding cold-boxes and read-out boxes will be mounted on C-shaped support frames. Each C-frame will carry a vertical and stereo half-layer. The modules of two C-frames closing around the beam-pipe form the detection layers. In total 6×2 C-frames will be arranged

Workpackage	C1	C2	C3	C4	C5	C6	C7
Mechanics	ok	ok	ok	ok	ok	ok	ok
Services: Water Novec Dry-Gas	 ok ok ok	 ok ok ok	 ok ok ok	 ok ok ok	 ok		 ok
Modules	ok	ok	ok	ok			
Heating	ok	ok	ok	i.p.			
Cabling	ok	ok	ok	ok	ok	ok	ok
Electronics	ok		ok				
Optical Fibres	ok		ok				
Commissioning	ok		i.p.				

Table 3: Status of the assembly and commissioning of the C-frames as of calender week 10. *ok* means concluded, *i.p.* means in progress.

along the beam-pipe. In addition to the mechanical support the 12 C-frames will also provide the necessary services to power, read-out and cooling of the detector elements.

The production of the mechanical components of all 12 C-frames is concluded and all parts have been delivered to CERN. The assembly of the first C-frames has started in early 2019 and meanwhile the mechanical structures of 7 C-frames have been completed. As next steps, cables, services, modules and the readout boxes are being installed on the mechanical structures. Table 3 summarizes the status for the first 7 C-frames (C1 to C7).

After assembly, the C-frames are cooled down to a temperature of $-40°$C on the cold-bars. This requires the operation of a cooling plant for the Novec, a stable vacuum insulation of all Novec lines, and, to prevent icing of the SiPMs, dry air flushing of the inner cold-box volume. For the C-frames which have been tested so far, the insulation vacuum reached a level of 10^{-4} mbar, sufficient to guarantee a good insulation of the Novec pipes. By flushing the cold-boxes with dry-gas a dew-point of $-50°$ in the cold-boxes was reached at a flow rate of 0.8 liter per hour. The cool-down to $-40°$C was smooth from the operational point of view. However, when $-40°$C were reached, water condensation on parts of the cold-boxes has been observed.

While the extent of the observed water built-up was largely related to the high humidity in the assembly hall during the 2019 summer, the observation of cold-spots on some parts of the cold-boxes was unexpected. X-ray studies in situ allowed us to trace back one of the problems to a mismatch between the lengths of the vacuum-insulating and the cold bellows, that could be prevented by a post-processing consisting essentially in a further stretching of the vacuum-insulating bellows. Further precautions were also taken to guarantee a safe operation in the experimental cavern: heating wires have been installed on the outside of the cold-boxes and also around the Novec bellows. The new heating system has been extensively tested for the first two C-frames. It has proven to avoid condensation and cold spots when the Novec cooling was operated at $-40°C$.

All other service systems (high-voltage and low-voltage supplies, data-acquisition system) have also been commissioned for C-frame C1. Readout tests at 40 MHz readout frequency have been performed for the installed readout boxes and a bit error rate smaller than 10^{-16} has been achieved. C-frame C1 is fully commissioned and has been moved to the transport and storage cage. The commissioning of C-frame C2 is in progress. Figure 10 shows the finished C-frame C1 when being moved into the transport and storage cage.

We expect to finish the first 6 C-frames until early summer 2020. The remaining ones eare expect to be finished in late autumn 2020. With respect to earlier schedules these dates are slightly delayed, mostly as a result of the mitigation measures necessary to avoid the condensation of water on cold-boxes and bellows.

Figure 10: Photograph of the first finished C-frame C1 when being moved to the transport and storage cage.

4.3.5 Preparation of detector installation

For the installation of the SciFi C-frames into the LHCb detector, the support mechanics of the former Outer Tracker had to be modified. The modification of the top and bottom rail system on the support bridge has been concluded. Cable trays and the distribution panels for Novec, water and dry gas are being installed. The cooling plant and the dry-gas system are well advanced. Before the installation of the C-frames, the cable chains need to be installed and filled with cables and pipes. The acquisition of the cable chains is delayed as the producers have difficulties to satisfy the CERN fire regulation. The manufacturing of the Novec transfer lines (vacuum insulated hoses to connect the C-frames to the distribution panels) is also slightly delayed.

To test the installation procedure, two C-frames (C-frame C7 and the prototype) have been transported to the cavern and have been successfully inserted onto the rails.

5 Status of upgrade: particle identification system

The Particle Identification (PID) system of the upgraded LHCb detector consists of the Ring-Imaging Cherenkov (RICH), Calorimeter and Muon systems. The design of the main components of the three sub-systems is complete. Mass production of several key detector and front-end electronics components is either complete or approaching completion. The projects are focusing on assembling the detector modules and electronics boards, installing in the pit at LHC Point 8 and commissioning. A more detailed summary of recent progress and plans for the next half year are given for each of the three sub-detectors of the PID system.

5.1 RICH system

The RICH detectors had been working extremely well in 2018 with no software or hardware issues to report. All the required maintenance took place during the YETS at the end of 2017. No further maintenance (see CERN-RRB-2018-099) was needed before the end of the year.

A complete Photon Detector Module (PDM) with its compliant DAQ was installed in RICH2 to take parasitic test data during the whole 2018 run. It was possible to detect light both synchronously and asynchronously with the LHC collisions and to get valuable experience with the Upgrade DAQ system and operation of the Upgrade front-end electronics. In particular, it allowed us, well in advance with respect to LHC Run 3, to discover and characterize an important mechanism (called Signal Induced Noise, SIN), which could have jeopardized the expected performance of the MaPMTs at 40 MHz. The process was understood, modelized and corrective actions have been taken to restore full system performance.

The following dismantling of the current detectors took place at the beginning of 2019, according to schedule, the radiator gases (CF_4 and C_4F_{10}) were carefully recuperated, in order not to impact the environment and the preparations for the reception of the new optoelectronic chains, optics and mechanics readied.

The upgraded RICH system consists of new photo-sensors with new front-end electronics that can be read out at 40 MHz, a re-designed RICH1 detector and RICH2. Simulations indicate that the physics performance of the new RICH system will be similar to that achieved with the existing detector in LHC Runs 1 and 2, albeit at a 10-fold high luminosity.

While RICH2 Optics remain in place and are the same as from 2005, RICH1 mirrors and transmission windows had to be modified, due to the new running conditions. Consequently, also the RICH1 gas enclosure had to be changed and adapted to the improved optical scheme. The carbon-fibre spherical mirrors and the glass flat mirrors for RICH1 have been both ordered and received. Both types of mirrors have undergone QA and characterization before being accepted. The quality is excellent. They will now go through a special coating process at CERN, which will provide them with a reflectivity expected in excess of 90% over the interested wavelength range.

After been produced and tested, the new RICH1 gas enclosure was installed on the beam line of LHCb in August 2019. However, shortly following its installation, one of its quartz window cracked, which led to an extensive and critical study of the incident and its consequences. Caring to not disrupt the overall LHCb schedule, solutions were found and are being applied. We expect to not intrude in the present LHCb schedule and be ready for re-installation in May.

The multi-anode photomultipliers (MaPMTs) are established as the technology for the RICH photon detector and are read out by a custom ASIC named CLARO. The order for the MaPMTs was placed in 2015, the pre-series has been delivered and was accepted in April 2016 after Quality Assurance (QA) tests. At this time, the full production was carried out and has been qualified. The MaPMT, CLARO, front-end electronics and system integration have been tested in test-beams and radiation areas. All results are satisfactory.

The photodetector arrays, including the MAPMTs, all on-detector electronics and ancillary systems, is common to RICH1 and RICH2. All components have gone through the production and QA phases for the RICH1 and RICH2 42+4 Columns and, in agreement with the schedule, the commissioning and installation of the whole photon detector has started at CERN. From single components to assembly and commissioned functional elements, a whole Quality Assurance process has been set-up and strictly followed in the last 2 years. Two laboratories at CERN have been set-up to test, characterize and study, and to commission in parallel single or multiple components. At this time, the whole A-side of RICH2 Photodetector Arrays has been fully commissioned and readied to be installed at the pit.

Important studies have been carried out to assess the compliance of all the electronic and mechanical components to the future hostile radiation environment. One important decision was the choice of the FPGA to adopt for the Digital Boards. Following these tests, we arrived to the conclusion that the Xilink Kintex7 is suitable for the RICH specifications and therefore we gave the green light for production and following QA to start. The full production and the specific QA for the Digital Boards is now finished, they are installed in the RICH2 and soon will be in the RICH1 Columns.

Finally, we are very sensitive to the environmental question and endeavoring to recuperate as much as possible of our radiator gases, both during beam operation as well as during maintenance, gas purification and filling operation. We are constantly improving our gas system, with the help of the support group EP-DT at CERN, and the leak tightness of our two gas vessels.

5.2 Calorimeter system

The upgrade of the calorimeter system consists in the replacement of the electromagnetic (ECAL) and hadronic (HCAL) calorimeter readout electronics and the removal of the Scintillating Pad Detector (SPD) and of the Preshower (PS).

The gain of the photomultipliers has been reduced by a factor up to five in order to keep them operational throughout the higher luminosity runs of the upgrade. The new analogue electronics partially compensates for the gain reduction by boosting signals by a factor of 2.5. The remaining factor 2 is used to extend the dynamics of the calorimeter system and thus to extend the physics case to some new topics. The upgraded detector will send the full data flow to the counting room at 40 MHz by means of four optical links per Front-End Board (FEB). The earliest-level trigger calculations are performed on the FEBs and the results are sent to the trigger farm in order to optimize the software trigger. The front-end electronics should be fully replaced. The high voltage, monitoring and calibration systems have been adapted to the new slow control based on the GBT driven optical links. The data-acquisition system relying on the PCIe40 boards is used, which requires a dedicated firmware adapted to the calorimeter data format.

5.2.1 Dismantling and installation in the cavern

The dismantling of the SPD, PS and of the lead absorber is completed. The lead sheet has been stored for a potential usage in the future. All the front-end boards and control boards in the crates at the pit have been removed, so that the racks are now ready to receive the new electronics. All unnecessary cables were also removed.

The Maraton power supplies that are needed to power up the crates have all been adapted to the new voltage/current configurations. The interconnections between the Maraton and the backplanes have been modified.

The long distance optical links have been passed from the surface down to the cavern and connected to the new general calorimeter patch panel recently installed behind the muon detector, close to the wall. Individual patch-panels have been installed on each crate of the ECAL and HCAL, on the platform, and connected to the general one by the semi-long fibres which have been passed above the muon detector. For that purpose, the cable trays above the muon spectrometer have been revisited.

 

Figure 11: Left: installation of the fibres between the new patch panel located beyond the muon spectrometer and the calorimeter platform. Right: an ECAL rack with its rack, emptied from its board and equipped, at the top, with a new patch panel, connected to the semi-long optical fibres.

The fibres connecting the front-end boards to the rack patch panels have been bought and are stored. They will be installed after the front-end boards are plugged.

The moving system of the calorimeter has been built in 2004. An overhaul of the six moto-reducers is planned and should be completed by mid-June. It will concern, the 4 moto-reducers of the two sides of the ECAL and HCAL and the two spare ones.

5.2.2 Production of electronic boards

The analogue electronics is based on an ASIC called ICECAL. The component has been produced in full quantity and tested. The design of the front-end board is now achieved, the performances are in specifications and we are waiting for the production of the boards. The plan is two receive 2, then 14 pre-production boards and finally the full production.

The two first pre-production boards are expected nowadays, but we are experiencing a delay from the company which is caused by two consecutive fabrication problems affecting the PCB and the schematics, respectively. These problems are now solved but caused a serious delay. The 16 pre-production boards should be tested in our laboratory before the green light is given for the fabrication of the full production that should last 11 weeks, 32 boards being delivered every week.

In the meantime and waiting for the production, the test programs have been developed. It was decided to move from a USB based test system to a test software written with WINCC (official control system of the experiment) so that a large fraction of the code necessary to control and monitor the calorimeter from the control room, in the future, is already available.

In order to speed up the test of the full production, the test benches have been doubled.

The control unit has reached also its final version. However, before launching the fabrication, it is preferable to realize a test in a fully loaded crate. Thus, the fabrication of the control units is postponed until the delivery of the 16 pre-production FEB. The control units will be cabled and delivered in three batches of 2, 12 and 12 boards. The delivery of the 2 pre-production boards is expected soon.

We plan to make a realistic test of the electronics, in the cavern, in April. A crate of the calorimeter platform will be equipped with the pre-production FEB and control boards connected to the already installed (see above) detector fibres. Our specific acquisition and control software will be installed on the LHCb farm computers that will be used for the test.

The high-voltage, monitoring and calibration systems have to be upgraded for two reasons. First, some mezzanines are too sensitive to radiation to bear the amount of particles that will be received during the upgrade data taking. Secondly, also the electronics has to be adapted to the new GBT based slow control system. A total of 144 new boards are needed, these include 132 mezzanines that will replace old ones on the mother boards. The mother boards are kept from the current system. The upgrade to the new slow control requires that 12 boards are made to convert the optical signal from the counting room into an electric signal that will feed some of the mezzanines.

All the boards have been produced and the post-production tests have been done successfully in Russia. A specific test bench has been developed for the functional tests and is now being used. At present 70% of the boards have been tested but less than a month is still necessary to test the remaining boards.

5.3 Muon system

The electronics of the Muon Detector Upgrade consists of a new readout board (nODE), equipped with four custom ASICs (nSYNC) redesigned to be compliant with a 40 MHz readout of the detector, and of new control boards, the Service Board (nSB) and the Pulse Distribution Module (nPDM), redesigned to be compliant with the new ECS/TFC system.

5.3.1 Status of the nSYNCs

The test and selection of all the needed nSYNCs (760) has been completed; 176 have already been installed on 44 nODE and the full set is at the company ready to be installed on the remaining nODE boards. Furthermore, about 100 additional spare nSYNCs has been selected for future usage.

5.3.2 Status of the nODE boards

The first pre-production of 24 nODE boards has been delivered and thoroughly tested in LNF in autumn 2019, showing only a fair yield: 18 out of 24 were fully working (problems being related mainly to the assembling process: soldering, component positioning, etc.). The production process has then been improved, and a second batch of 20 boards showed a much better yield: 19 out of 20 were correctly working. The production has started and, at present, we expect the full production to be delivered at CERN in few batches from April to June 2020.

5.3.3 Status of the nSB and nPDM boards

All the needed nSB (140) and nPDM boards (8) have been delivered and tested in Roma1. They will be installed on the apparatus in March.

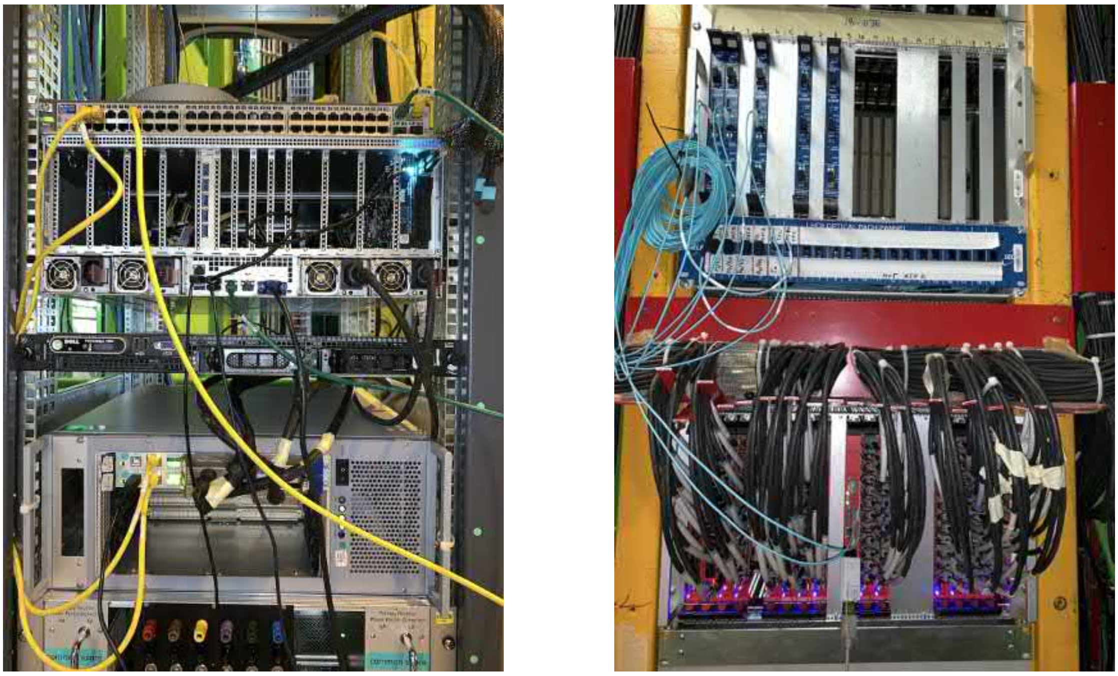

Figure 12: The Muon commissioning rack (left) and the Q1M45 Muon rack (right), fully equipped with new readout and control electronics

5.3.4 Commissioning

The commissioning phase will be split in two parts: in the first part we will check the connectivity between the chambers and the nODEs by pulsing the FEBs and reading back the signals on the PCIe40 readout board. In the second part, once the online farm will be available, the signals will be readout form the data center using the standard readout chain.

The first connectivity test has been done on the first quadrant of station M4, using the "Muon commissioning rack", which contain two primary power supplies, to power up the two Maratons in the Muon rack, and a PCIe40 readout card (configured as SOL40), to communicate with the electronics (see fig. 12). This was primarily aimed to finalize and debug the nODE-nSB configuration libraries and the new ECS software. We are now installing the nODEs in other regions (e.g. Q4M4) and starting the systematic test of the full detector. The plan is to have the detector completely equipped with the new electronics by the summer, and to complete the test by the end of 2020.

In parallel, also the activities related to the additional material in front of M2, foreseen to reduce by about a factor 2 the low energy background rate in this region (see Fig.13), are progressing . The Tungsten slabs, to be installed in place of the inner-most cells of HCAL, were delivered at CERN in April 2019, and are ready to be installed. The new HCAL Beam Plugs, with an improved beam-pipe inner profile (will go one cm closer to the beam pipe), were delivered and installed. The new M2 beam plug, where part of the Steel was replaced with Lead, have been delivered and will be installed in the next weeks.

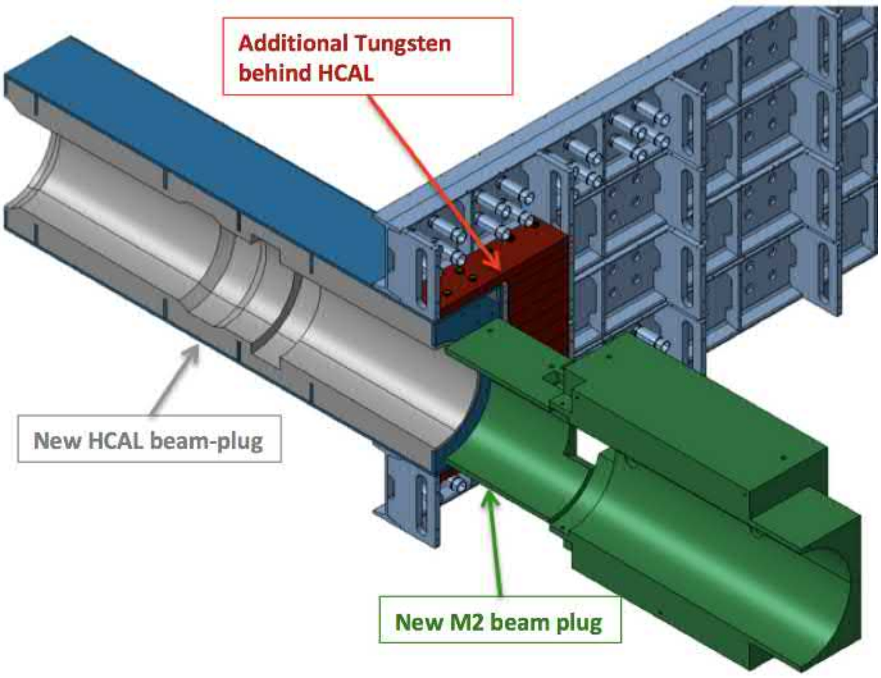

Figure 13: Schematic view of the HCAL and M2 Beam Plugs, and the additional Tungsten in place of the inner-most HCAL Cells

6 Status of upgrade: fixed target (SMOG2)

LHCb is the only experiment at the Large Hadron Collider (LHC) that can take data both in collider and fixed-target mode. The LHCb fixed-target system, called SMOG (System for Measuring the Overlap with Gas) [49] allows to inject a low rate of noble gases into the vacuum vessel of VELO. This gives the unique opportunity to operate an LHC experiment in fixed-target mode, and to study proton-nucleus and nucleus-nucleus collisions on various target types and at different center-of-mass energies (see CERN-RRB-2019-037 and section 3).

An upgrade of the SMOG system, SMOG2 [50], has been installed during the LS2. The main element of SMOG2 is a storage cell for the injected gas (Fig. 14), to be installed at the upstream edge of the VELO, coaxial with the LHC beam, displaced of 30 cm from the main interaction point. One of the main advantages of SMOG2 is the possibility to reach much higher effective areal densities (and thus luminosities) with respect to SMOG at the same injected gas flux. A detailed

Figure 14: SMOG2 storage cell half with wake field suppressor, attached to a VELO RF box during the pre-installation mounting.

physics programme with a fixed target at LHCb has been presented in a dedicated report of the Physics Beyond Colliders study group in Ref. [51].

The TDR has been approved by the LHCC [50] and all machine aspects have been discussed several times in LHC dedicated meetings, in particular within the vacuum group, at the LHC Tunnel Region Experiments Working Group (TREX), at the LHC Machine Protection Panel (MPP), and at the LHC Machine Committee (LMC) meetings. A dedicated Engineering Design Review was held in November

2018 and an Engineering Change Request (ECR) has been approved by the LMC committee. After the installation of the storage cell, the other key component of SMOG2 is the Gas Feed System, now in its assembling and calibration phase. By this system it will be possible to inject precise fluxes of gas, from hydrogen to heavy noble gases, that, together with the input from five temperature probes installed along the storage cell, will give a very precise measurement of the instant luminosity. Software and trigger implementations are already well advanced. Preliminary studies show that it is possible to run simultaneously in pp and p-gas mode without loosing reconstruction efficiency nor data to storage flow.

7 Status of upgrade: online, trigger and real-time analysis, computing

7.1 Online

The heart of the online system is the event-builder, which assembles the event at a rate of 40 MHz. The design relies on a large bandwidth bi-directional network interconnecting the event-builder PC-servers and on a generic (PCI Express) readout module, the PCIe40 board, embedded in each PC-Server.

The production of 911 PCIe40 modules is performed via a CERN contract for both LHCb and ALICE Collaborations. The production was launched at the end of January 2019. The last module was delivered in March 2020. An ultimate batch of 358 modules was ordered in October 2019, mainly for the ALICE collaboration. The delivery is scheduled between April and June 2020.

An a exhaustive qualification procedure was run on hardware provided by different vendors, in order to select the PC-server for the event-builder. The order of 200 PC-servers was launch end November 2019. Their delivery is foreseen in April 2020 at the earliest due to the covid-19 outbreak.

The event-builder has to aggregate 40 Tbits/s. The baseline architecture relies on a 200 Gbits/s bi-directional network interconnecting PC-servers. In December, the decision was taken on the event-builder architecture. Each PC-server hosts three PCIe40 modules and two interfaces running at 200 Gbits/s each. The tender for the network was launched in February 2020. Installation will be completed by August 2020, if there are no further delays on the shipments on top of the 8 weeks already incurred.

A platform for integration and performance tests is running since October 2018 at the surface of LHC Point 8. It is used for full scale test of the *Timing and Fast Control* chain, develop the event-builder software and test new ideas based on GPU or FPGA co-processors.

To house the event-builder and the event-filter farm, a new data centre has been built on the surface at the LHCb experimental site. It is composed of six containers located at LHC Point 8. They are fully operational since November 2019. Two containers are used by CERN-IT since mid 2019. A large part of the old LHCb farm, used during Run 2, migrated as well as the platform for integration and performance tests. The current power consumption is around 1 MW.

The surface and the underground areas are connected via a backbone of long distance optical cables. The installation of the 19008 long distance optical fibres ended in September 2019. Short distance optical cables interconnect long distance ones to PC-servers within data centre. The ECS connectivity will be ready by end of March and the DAQ one in June.

Full data acquisition system will be ready for detector commissioning by October 2020.

7.2 Trigger and real-time analysis

The Upgrade trigger [6] consists of a collection of identical software tasks running on the event-filter farm. All collisions are reconstructed in real time with the best possible quality and then selected to be written for offline storage. This process is done in two steps. In the first one, HLT1, the fast reconstruction sequence is run in order to reduce the rate to about 1 MHz. Data are then stored locally waiting for the calibration and alignment constants. Once ready, the second step, HLT2, performs the full reconstruction and selects collisions interesting for the physics. In this scheme, the full reconstruction is done once and never redone at later stages.

In order to reach this ambitious goal, the collaboration created the *Real Time Analysis* project. It is organized like a detector project and it is supervised by the Technical Board. The project is organized in six working groups covering data structures, reconstruction, calibration and alignments, selections, quality assurance as well as the possible use of accelerators. It works in close collaboration with the Online and Computing projects. The organization of the project is in place since January 2019.

The project reached the state where the fast reconstruction can process 30 MHz of collisions when running on a thousand reference servers equipped with x86 CPU.

The full reconstruction is working in the new framework. The throughput increased by about 50% to reach 137 kHz, in past months. Work on the event model and on critical algorithms have to continue in order to improve throughput preserving efficiencies and precision. Finally, the layer combining particles has to be implemented as well as many lines to select collisions interesting for the physics.

Partial and full reconstruction have to be ready by Q3 2020.

In parallel, the fast reconstruction has been ported to an heterogeneous architecture in which CPU uses GPU co-processor. The *Allen* proposal is described in TDR-like document covering all aspects of such projects. It is supported by 14 institutes at level of 20 FTE. The document was submitted to the collaboration end January 2020. It shows that the Allen project fully satisfied requirements of the LHCb Collaboration for fast processing. The collaboration setup a review committee which shall provide a recommendation by end of March.

7.3 Computing

Activities in the core software domain were focused in the areas of conditions data and detector description, in order to make them compliant with thread safety and concurrency.

In the last few months, the prototype of the integration of DD4HEP in the LHCb software stack was finalised. It demonstrates how to use this toolkit, from the definition of the geometry to the use of conditions in the LHCb functional algorithm framework. It integrates the GITCONDDB library to load conditions, as well as a recent version of the DD4HEP toolkit in which the LHCb VeloPixel and SciFi detectors have been ported. Working is currently ongoing to merge these features into the main branch of the LHCb code.

Significant efforts were spent to prepare a tutorial that illustrates how to add sub-detectors and create the associated conditions, which was very useful as training during the LHCb Upgrade Software hackathon held in February 2020.

During the hackathon, efforts started to port other sub-detectors to DD4HEP, *e.g.* the Muon chambers, as well as to provide tools to compare the current LHCb geometry (DETDESC) with the port to DD4HEP.

LHCb is continuing its efforts to modernise its software stack, migrating as aggressively as possible to new compilers. As an example, gcc 9 is now used for software releases. In order to ease development, a refactoring of the continuous integration tools is also under way. The goal is to test each merge request individually while only reconstructing the parts of the stack which have changed.

Regarding distributed computing, within the last six months the LHCbDIRAC team spent a considerable effort in sorting out several technical tasks, including the migration of DIRAC services from SLC6 to new CentOS7 VOboxes, using newly-developed puppet templates, and fully adopting DIRACOS, a *container-like* solution for DIRAC requirements. Another accomplished technical task was the development and adoption of a comprehensive automated test infrastructure, and the automation of releases deployment. The team is also preparing the updates of databases such as MySQL, Oracle, and ElasticSearch to their newest releases. The first steps towards the adoption of CentOS8 have also been done. At the same time, the DIRAC and LHCbDIRAC code is being slowly but steadily moving to python 3, with the DIRAC pilots now being fully compatible with python 2 and 3.

The LHCbDIRAC team has also certified a DIRAC release that will allow an easier exploitation of non-standard Grid resources. The required features include full support for multi-processor jobs and resources, including support for intra-node partitioning. The team is also deploying a DIRAC release that includes a better integration of computing resources exposing the SLURM batch system, which is the one typically adopted in HPC centers.

8 Status of upgrade: infrastructure

After the successful dismantling of the old detector systems, an intense phase of overhauling of several services and infrastructures is currently going on. This involves both the global experiment services and specific infrastructure for subdetectors. The installation phase is also in full swing, coordinated by the Technical Coordination team.

8.1 Infrastructure

All detector cooling systems are now in the commissioning phase, with detectors being bypassed, although the manifolds for the SciFi system (for the SiPMs and Front-End electronics) remain to be installed. Problems of leaking valves in the Novec cooling systems were identified and are being addressed by the manufacturer.

The CO2 cooling systems for the VELO and Upstream Tracker were contaminated by silicon oil, which was traced back as originating from pressure sensors. Sensors will be replaced and the circuits will need a thorough cleaning. The commissioning of the detector cooling system was planned to be completed by April 2020.

The VELO and RICH HV cables delivered were found to be not compliant with the CERN safety regulations. New cables were delivered in batches since Q3 2019 and the subsequent delays were mitigated by reshuffling the installation sequence. All long distance cables which were foreseen to be installed are now in place, within one month of the original schedule. It is anticipated that requests for new cables will arise during LS2 or even later. Cables delivered before the closure of the shielding wall in spring 2020 will be installed immediately. Provision for the installation of a small subset of additional cables after LS2 has been made by installing feed through ducts.

The supporting rails and the guiding system for the SciFi stations have been installed and aligned. The access platforms of the former Outer Tracker have been modified and moved for the purpose of accessing the ScFi Front-End electronic boxes. The guiding system and supports for the cable chains have been produced and are being installed. The supports for UT service bays have been welded and the access platforms were modified to allow PEPI electronics installation. The control of the VELO vacuum system has been commissioned and the HV patch panels installed. New survey reference points were installed to align the SMOG2 storage cell in situ.

8.2 Installation

The SMOG2 gas storage cell has been assembled and pre-aligned with respect to the VELO RF-box. The installation of the RF-box in the VELO was ready to take

Figure 15: Transport of the prototype SciFi C-frame and one a final empty C-frame for test reason.

place in the first half of March 2020 but had to be postponed because of travel restrictions applying to the personnel of participating institutes.

The RICH-1 gas enclosure that was pre-installed at the end of 2019, had to be taken out of its position as a crack in the quarts window appeared spontaneously after installation. A new quartz window has been ordered. The gas enclosure was shipped to Oxford in order to improve the gas tightness and the overall stiffness of the chamber. It is foreseen to have the gas enclosure ready for installation in late May 2020.

A dry tests of the SciFi C-frame installation was performed. Two C-frames (without modules) were lowered and installed in their final position (Fig.15). The tooling and installation procedure are ready for the installation of the fully equipped C-frames.

A rack has been fully equipped with the new read-out electronics of the Muon system and it is being commissioned. The additional shielding elements to be placed in front of the Muon M2 station are ready for installation and alignment.

9 Status of upgrade: project organization

9.1 Project organization

The upgrade activity is overseen by the Upgrade Detector Planning Group (UDPG). The UDPG membership consists of an Upgrade Coordinator (chair), an Upgrade Resources Coordinator, an Upgrade Data Processing Coordinator, an Upgrade Electronics Coordinator, as well as the management and a representative of the Physics Coordinator.

All the activities concerning the development of the all-software trigger are coordinated by the Upgrade Software Planning Group (USPG). The USPG membership consists of the USPG chair, representatives of the Computing, Online and Real-Time Analysis projects and of the Simulation working group, the Operation Coordinator, as well as the management and the physics coordination team.

The UDPG and USPG meet regularly to review progress of the various projects. Detector and software upgrade activities are organised within the existing Projects and working groups, to ensure efficient sharing of resources between operational needs and Upgrade work.

9.2 Milestones

Three major milestones have been achieved in the last six months, most notably in the UT project with the successful completion of the silicon sensor and data flex cable productions (see section 4.2) and the Online project, with the decision on the readout network technology and the completion of the PCIe40 board production (see section 7).

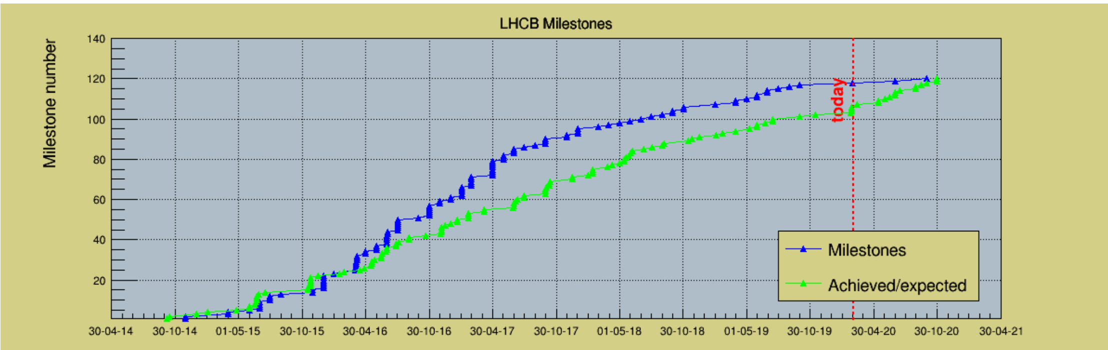

Figure 16: Snapshot of LHCb Upgrade milestones.

A snapshot of the global status is given in Fig. 16. The overall delay of around six to twelve months with respect to original planning is mostly absorbed in the foreseen contingency and in the extension of the LS2 duration. Progress continues at a steady pace. Overall, the Upgrade project is on track for completion and installation in LS2. Most subdetectors are under construction and in line with the installation schedule. Some areas of concern are being closely monitored (in particular UT and VELO) and actions have been taken to mitigate the delays. It was decided that the UT detector project would not be installed before the beam pipe. Therefore, tooling and procedures are being developed for a delayed arrival in LS2.

After installation, the full detector will need to be commissioned and steps have been taken to prepare this phase. The commissioning coordinator is organizing regular commissioning meetings and all subdetector projects are making good progress.

9.3 Funding

For the present M&O Cat.A and B, the status of the accounts is healthy and no cash flow problems are foreseen if all members will contribute timely to the budget. The expenditure on the 2019 M&O Cat.A budget followed well our forecasts. Year 2019 and first LS2 activity year, is well balanced, thanks also to the financial plan (M&O Cat.A levels for the forthcoming LS2 and successive upgrade phase) which we finalised, submitted and got approved by the Scrutiny Group and by the RRB in 2017 and 2018. This plan foresaw an increase in the budget for 2019 to 2.725 MCHF plus the help of 0.4 MCHF of pluriannual surplus. A smooth transition is requested to the sub-detectors projects for their M&O Cat.B. This seems to be happening nicely, although it remains clear the difficulty of estimating resources and technical commitments for the completely new sub-detectors.

The funding requirements for the LHCb Upgrade construction have been defined in detail in Addendum No. 1 to the Memorandum of Understanding (MoU) for Common Projects [9] and in the Addendum No. 2 to the MoU for the Upgrade of the Sub-Detector Systems [10], which refer to the LHCb Upgrade Framework Technical Design Report (FTDR) [2] and the Technical Design Reports (TDRs) for all Upgrade sub-detector systems [3–8]. These documents define in all details the technical design and cost of the upgraded detector, as well as the sharing of responsibilities among the institutes and Funding Agencies in the construction, installation and commissioning of the upgraded sub-systems. The total cost of the LHCb Upgrade of 57.2 MCHF is divided into Common Projects for an amount of 15.7 MCHF and Sub-Detector Projects for an amount of 41.5 MCHF.

At present, the LHCb Upgrade project continues to progress as planned. All major contracts have been placed and spending of CORE funds is proceeding for all of the sub-detector components. Most of the remaining funds for sub-detectors construction have been spent in 2019. The majority of the Common Project funds (in particular for the acquisition of the Computing Farm) are expected to be spent in 2020-2021. The Upgrade project continues to evolve within the agreed cost envelope and there is confidence that the funding profile will match the spending profile to ensure a complete and timely installation of the new experiment by the end of LS2.

10 Upgrade II

A timescale has been agreed by the LHCC for submission of the Framework TDR for Upgrade II. As previously reported a physics case document was submitted in 2018 and presented to the LHCC [52] along with a document prepared by the HL-LHC team who have studied the options for delivering the required luminosity for the LHCb Upgrade II [53]. The framework TDR will be submitted in 2021. This will be followed by subsystem TDRs describing consolidation in LS3 and later by subsystem TDRs describing the Upgrade II for LS4. The RRB will be kept fully informed of the preparation of these documents.

The LHCb Upgrade II was extensively discussed in the European Strategy for Particle Physics Update Symposium, held in Granada in May 2019. The particle physics community was strongly supportive of the LHCb Upgrade II.

R&D on Upgrade II is active across all sub-detectors. A number of the contributing nations have funded programmes with relevance to Upgrade II. Internal notes have been produced and reviewed in the spring for subsystems aiming for installation during the LS3 consolidation phase. The same process is now being performed over the next months for full Upgrade II subdetectors.

The HL-LHC project have established an organisation for the accelerator studies required for Upgrade II. This group has made site visits to LHCb and excellent collaboration has been established wth LHCb. The HL-LHC team will prepare a Conceptual Design Report for the machine modifications on the same timescale as the Framework TDR.

The fifth in the sequence of dedicated workshops on Upgrade II is taking place in Barcelona in spring 2020 and, in light of the positive LHCC recommendation, will focus on the preparations for the Framework TDR.

11 Collaboration matters

Four new groups joined the collaboration as associate members: Helmholtz-Institut für Strahlen-und Kernphysik (HISKP) at Bonn University (Bonn, Germany), La Salle-Universitat Ramon Llull (Barcelona, Spain), Maastricht University (Maastricht, The Netherlands), INFN and University of Perugia (Perugia, Italy).

References

[1] *Letter of Intent for the LHCb Upgrade*, CERN-LHCC-2011-001. LHCC-I-018, 2011.

[2] LHCb collaboration, *Framework TDR for the LHCb Upgrade: Technical Design Report*, CERN-LHCC-2012-007, 2012.

[3] LHCb collaboration, *LHCb VELO Upgrade Technical Design Report*, CERN-LHCC-2013-021, 2013.

[4] LHCb collaboration, *LHCb PID Upgrade Technical Design Report*, CERN-LHCC-2013-022, 2013.

[5] LHCb collaboration, *LHCb Tracker Upgrade Technical Design Report*, CERN-LHCC-2014-001, 2014.

[6] LHCb collaboration, *LHCb Trigger and Online Technical Design Report*, CERN-LHCC-2014-016, 2014.

[7] LHCb collaboration, *LHCb Upgrade Software and Computing*, CERN-LHCC-2018-007, 2018.

[8] LHCb collaboration, *Computing Model of the Upgrade LHCb experiment*, CERN-LHCC-2018-014, 2018.

[9] LHCb collaboration, *Addendum No. 01 to the Memorandum of Understanding for Collaboration in the Construction of the LHCb Detector. The Upgrade of the LHCb Detector: Common Project items*, CERN-RRB-2012-119A, revised April 2014, 2012.

[10] LHCb collaboration, *Addendum No. 2 to the Memorandum of Understanding for Collaboration in the Construction of the LHCb Detector Upgrade of the LHCb detector Sub-Detector Systems*, CERN-RRB-2014-105, 2014.

[11] C. Bozzi, *LHCb Computing Resource usage in 2019*, Tech. Rep. LHCb-PUB-2020-002. CERN-LHCb-PUB-2020-002, CERN, Geneva, 2020.

[12] C. Bozzi, *LHCb Computing Resources: update of 2021 requests*, Tech. Rep. LHCb-PUB-2020-001. CERN-LHCb-PUB-2020-001, CERN, Geneva, 2020.

[13] C. M. LHCb Collaboration, *Computing Model of the Upgrade LHCb experiment*, Tech. Rep. CERN-LHCC-2018-014. LHCB-TDR-018, CERN, Geneva, 2018.

[14] LHCb collaboration, R. Aaij *et al.*, *Updated measurement of decay-time-dependent CP asymmetries in $D^0 \to K^+K^-$ and $D^0 \to \pi^+\pi^-$ decays*, Phys. Rev. **D101** (2020) 012005, `arXiv:1911.01114`.

[15] LHCb collaboration, R. Aaij *et al.*, *Measurement of CP violation in $B^0 \to D^{*\pm}D^{\mp}$ decays*, `arXiv:1912.03723`, submitted to JHEP.

[16] LHCb collaboration, R. Aaij *et al.*, *Measurement of CP observables in $B^\pm \to DK^\pm$ and $B^\pm \to D\pi^\pm$ with $D \to K^0_S K\pi$ decays*, LHCb-PAPER-2019-044 CERN-EP-2020-015, in preparation.

[17] CLEO, J. Insler *et al.*, *Studies of the decays $D^0 \to K^0_S K^-\pi^+$ and $D^0 \to K^0_S K^+\pi^-$*, Phys. Rev. **D85** (2012) 092016, `arXiv:1203.3804`, [Erratum: Phys. Rev.D94,no.9,099905(2016)].

[18] LHCb collaboration, R. Aaij *et al.*, *A study of CP violation in $B^\pm \to DK^\pm$ and $B^\pm \to D\pi^\pm$ decays with $D \to K^0_S K^\pm\pi^\mp$ final states*, Phys. Lett. **B733** (2014) 36, `arXiv:1402.2982`.

[19] LHCb collaboration, R. Aaij *et al.*, *Measurement of $|V_{cb}|$ with $B^0_s \to D_s^{(*)-}\mu^+\nu$ decays*, `arXiv:2001.03225`, submitted to Phys. Rev. D.

[20] I. Caprini, L. Lellouch, and M. Neubert, *Dispersive bounds on the shape of anti-B —¿ D(*) lepton anti-neutrino form-factors*, Nucl. Phys. **B530** (1998) 153, `arXiv:hep-ph/9712417`.

[21] C. G. Boyd, B. Grinstein, and R. F. Lebed, *Precision corrections to dispersive bounds on form-factors*, Phys. Rev. **D56** (1997) 6895, `arXiv:hep-ph/9705252`.

[22] LHCb collaboration, R. Aaij *et al.*, *Search for CP violation and observation of P violation in $\Lambda_b^0 \to p\pi^-\pi^+\pi^-$ decays*, `arXiv:1912.10741`, submitted to PRL.

[23] LHCb collaboration, R. Aaij *et al.*, *Test of lepton universality using $\Lambda_b^0 \to pK^-\ell^+\ell^-$ decays*, `arXiv:1912.08139`, submitted to JHEP.

[24] LHCb collaboration, R. Aaij *et al.*, , LHCb-PAPER-2020-002, in preparation.

[25] LHCb collaboration, R. Aaij *et al.*, *Search for the lepton flavour violating decay $B^+ \to K^+\mu^-\tau^+$ using B_{s2}^{*0} decays*, LHCb-PAPER-2019-043 CERN-EP-2020-020, in preparation.

[26] LHCb collaboration, R. Aaij *et al.*, , LHCb-PAPER-2020-001, in preparation.

[27] LHCb collaboration, R. Aaij *et al.*, *Strong constraints on the $K_S^0 \to \mu^+\mu^-$ branching fraction*, `arXiv:2001.10354`, submitted to PRL.

[28] LHCb collaboration, R. Aaij *et al.*, *Observation of the semileptonic decay $B^+ \to p\overline{p}\mu^+\nu_\mu$*, `arXiv:1911.08187`, submitted to JHEP.

[29] LHCb collaboration, R. Aaij *et al.*, *Isospin amplitudes in $\Lambda_b^0 \to J/\psi\,\Lambda(\Sigma^0)$ and $\Xi_b \to J/\psi\,\Xi^0(\Lambda)$ decays*, `arXiv:1912.02110`, submitted to PRL.

[30] G. Hiller, M. Jung, and S. Schacht, *SU(3)$_F$ in nonleptonic charm decays*, PoS **EPS-HEP2013** (2013) 371, `arXiv:1311.3883`.

[31] A. Dery, M. Ghosh, Y. Grossman, and S. Schacht, *SU(3)$_F$ Analysis for Beauty Baryon Decays*, `arXiv:2001.05397`.

[32] LHCb collaboration, R. Aaij *et al.*, *Measurement of the branching fraction of the decay $B_s^0 \to K_S^0 K_S^0$*, LHCb-PAPER-2019-030, in preparation.

[33] LHCb collaboration, R. Aaij *et al.*, *Determination of quantum numbers for several excited charmed mesons observed in $B^- \to D^{*+}\pi^-\pi^-$ decays*, `arXiv:1911.03326`.

[34] LHCb collaboration, R. Aaij *et al.*, *First observation of excited Ω_b^- states*, `arXiv:2001.00851`, submitted to Phys. Rev. Lett.

[35] LHCb collaboration, R. Aaij *et al.*, *Observation of five new narrow Ω_c^0 states decaying to $\Xi_c^+ K^-$*, Phys. Rev. Lett. **118** (2017) 182001, arXiv:1703.04639.

[36] LHCb collaboration, R. Aaij *et al.*, *Observation of a new baryon state in the $\Lambda_b^0\pi^+\pi^-$ mass spectrum*, arXiv:2002.05112, submitted to JHEP.

[37] LHCb collaboration, R. Aaij *et al.*, *Observation of excited Λ_b^0 baryons*, Phys. Rev. Lett. **109** (2012) 172003, arXiv:1205.3452.

[38] LHCb collaboration, R. Aaij *et al.*, *Observation of new resonances in the $\Lambda_b^0\pi^+\pi^-$ system*, Phys. Rev. Lett. **123** (2019) 152001, arXiv:1907.13598.

[39] LHCb collaboration, R. Aaij *et al.*, *Measurement of Ξ_{cc}^{++} production in pp collisions at $\sqrt{s} = 13$ TeV*, Chin. Phys. C **44** (2020) 022001, arXiv:1910.11316.

[40] LHCb collaboration, R. Aaij *et al.*, *Precision measurement of the Ξ_{cc}^{++} mass*, JHEP **02** (2020) 049, arXiv:1911.08594.

[41] LHCb collaboration, R. Aaij *et al.*, *Search for the doubly charmed baryon Ξ_{cc}^+*, Sci. China Phys. Mech. Astron. **63** (2020) 221062, arXiv:1909.12273.

[42] LHCb collaboration, R. Aaij *et al.*, *Measurement of f_s/f_u variation with proton-proton collision energy and kinematics*, arXiv:1910.09934, submitted to Phys.Rev.Lett.

[43] LHCb collaboration, R. Aaij *et al.*, *Measurement of the B_c^- production fraction and asymmetry in 7 and 13 TeV pp collisions*, Phys. Rev. **D100** (2019) 112006, arXiv:1910.13404.

[44] LHCb collaboration, R. Aaij *et al.*, *Measurement of the $\eta_c(1S)$ production cross-section in pp collisions at $\sqrt{s} = 13$ TeV*, arXiv:1911.03326, submitted to EPJC.

[45] LHCb collaboration, *Measurement of the Z production cross-sections in pPb collisions at $\sqrt{}$=8 TeV*, LHCb-CONF-2019-003, 2019.

[46] LHCb collaboration, *Study of prompt D^0 meson production in p Pb at $\sqrt{s_{\mathrm{NN}}}$ = 8.16 TeV at LHCb*, LHCb-CONF-2019-004, 2019.

[47] LHCb collaboration, *Multiplicity-dependent modification of $\chi_{c1}(3872)$ and $\psi(2S)$ production in pp collisions at $\sqrt{s} = 8$ TeV*, LHCb-CONF-2019-005, 2019.

[48] LHCb collaboration, R. Aaij *et al.*, *Search for $A' \to \mu^+\mu^-$ decays*, Phys. Rev. Lett. **124** (2020) 041801, arXiv:1910.06926.

[49] M. Ferro-Luzzi, *Proposal for an absolute luminosity determination in colliding beam experiments using vertex detection of beam-gas interactions*, Nucl. Instrum. Meth. **A553** (2005) 388.

[50] LHCb collaboration, *LHCb SMOG Upgrade*, CERN-LHCC-2019-005, 2019.

[51] A. Bursche *et al.*, *Physics opportunities with the fixed-target program of the LHCb experiment using an unpolarized gas target*, Tech. Rep. LHCb-PUB-2018-015. CERN-LHCb-PUB-2018-015, CERN, Geneva, 2018.

[52] LHCb collaboration, *Physics case for an LHCb Upgrade II — Opportunities in flavour physics, and beyond, in the HL-LHC era*, `arXiv:1808.08865`.

[53] I. Efthymiopoulos *et al.*, *LHCb Upgrades and operation at 1034 cm-2 s-1 luminosity –A first study*, Tech. Rep. CERN-ACC-NOTE-2018-0038, CERN, Geneva, 2018.